JCI insight

RESEARCH ARTICLE

Cannabinoid CB_1 receptor overactivity contributes to the pathogenesis of idiopathic pulmonary fibrosis

Resat Cinar,[1] Bernadette R. Gochuico,[2] Malliga R. Iyer,[1] Tony Jourdan,[1] Tadafumi Yokoyama,[2] Joshua K. Park,[1] Nathan J. Coffey,[1] Hadass Pri-Chen,[2] Gergő Szanda,[1] Ziyi Liu,[1] Ken Mackie,[3] William A. Gahl,[2] and George Kunos[1]

[1]Laboratory of Physiologic Studies, National Institute on Alcohol Abuse and Alcoholism (NIAAA), and [2]Medical Genetics Branch, National Human Genome Research Institute, NIH, Bethesda, Maryland, USA. [3]Department of Psychological and Brain Sciences, Indiana University, Bloomington, Indiana, USA.

Idiopathic pulmonary fibrosis (IPF) is a life-threatening disease without effective treatment, highlighting the need for identifying new targets and treatment modalities. The pathogenesis of IPF is complex, and engaging multiple targets simultaneously might improve therapeutic efficacy. To assess the role of the endocannabinoid/cannabinoid receptor 1 (endocannabinoid/CB_1R) system in IPF and its interaction with inducible nitric oxide synthase (iNOS) as dual therapeutic targets, we analyzed lung fibrosis and the status of the endocannabinoid/CB_1R system and iNOS in mice with bleomycin-induced pulmonary fibrosis (PF) and in lung tissue and bronchoalveolar lavage fluid (BALF) from patients with IPF, as well as controls. In addition, we investigated the antifibrotic efficacy in the mouse PF model of an orally bioavailable and peripherally restricted CB_1R/iNOS hybrid inhibitor. We report that increased activity of the endocannabinoid/CB_1R system parallels disease progression in the lungs of patients with idiopathic PF and in mice with bleomycin-induced PF and is associated with increased tissue levels of interferon regulatory factor-5. Furthermore, we demonstrate that simultaneous engagement of the secondary target iNOS by the hybrid CB_1R/iNOS inhibitor has greater antifibrotic efficacy than inhibition of CB_1R alone. This hybrid antagonist also arrests the progression of established fibrosis in mice, thus making it a viable candidate for future translational studies in IPF.

Introduction

Fibrosis is a highly prevalent, multifactorial, and progressive pathogenic process affecting many organs, including the lungs (1). Pulmonary fibrosis (PF) is a life-threatening disease that may benefit from simultaneously targeting multiple pathways to improve therapeutic efficacy. Combination therapy can achieve this, but its practicality is often limited by complicated pharmacokinetics and dosing schedules as well as extensive drug-drug interactions and adverse effects (2). Indeed, clinical trials using combination therapies for idiopathic PF (IPF) have yielded disappointing results, showing lack of efficacy or even worsening outcomes (3). Although the FDA recently approved pirfenidone and nintedanib for the treatment of IPF, both compounds have tolerability problems, modest efficacy, and poor pharmacokinetic properties in clinical use (4, 5). Polypharmacology is an emerging strategy that involves the use of a single chemical entity to target multiple therapeutic pathways (6). A rational application of polypharmacology in the case of IPF may involve simultaneously targeting distinct pathways affecting alveolar inflammation and the fibrotic process itself. For instance, a pathway regulating redox balance together with any other profibrotic pathway might be a rational target for polypharmacology, in view of the dysregulation of oxidant/antioxidant balance in fibrotic disorders, including IPF, resulting in increased production of reactive oxygen and nitrogen species, which likely contribute to respiratory failure and poor survival (7, 8).

Inducible nitric oxide synthase (iNOS) catalyzes the generation of inflammatory reactive nitrogen species involved in cell injury. iNOS is induced in fibrotic lung tissues in mice (9, 10) and humans (11), and the early proliferative response of human pulmonary fibroblasts to inflammatory stimuli is associated with increased iNOS gene expression (12). iNOS protein levels are strongly correlated with the degree of PF in human lung

Conflict of interest: R. Cinar, M.R. Iyer, and G. Kunos are listed as coinventors on a US patent application (PCT/US2013/069686) covering MRI-1867 and related compounds.

Submitted: December 13, 2016
Accepted: March 7, 2017
Published: April 20, 2017

Reference information:
JCI Insight. 2017;2(8):e92281. https://doi.org/10.1172/jci.insight.92281.

tissue, and low expression of iNOS is associated with reduced risk of death (13). Furthermore, iNOS inhibitors have antifibrotic activity in animal models of PF (14, 15), making iNOS a viable therapeutic target for PF.

The endocannabinoid/cannabinoid receptor 1 (endocannabinoid/CB_1R) system is another rational therapeutic target in PF. Endocannabinoids are bioactive lipids that act on cannabinoid receptors, CB_1R and CB_2R, that also recognize and mediate the effects of marijuana (16). Endocannabinoids acting via CB_1R promote fibrosis progression in multiple organs, including liver (17–21), kidney (22, 23), heart (24), and skin (25), and CB_1R has been linked to radiation-induced PF in mice (26). In addition to promoting fibrosis, activation of CB_1R is proinflammatory in chronic inflammatory diseases (27, 28), whereas the brain-penetrant CB_1R antagonist/inverse agonist rimonabant mitigates liver fibrosis in animal models (17). However, the potential role of CB_1R in IPF has not yet been investigated either in the human disease or in an animal model.

Here, we evaluated the role of the endocannabinoid/CB_1R system and iNOS in human IPF and in the bleomycin-induced mouse model of PF (BL-PF). Our observations point to an overactivity of both the endocannabinoid/CB_1R system and iNOS, as assessed in bronchoalveolar lavage fluid (BALF) and lung tissue from both human subjects with IPF and mice with BL-PF as well as their respective controls. We also provide evidence that one of the downstream mediators of CB_1R activation in the fibrotic lung is interferon regulatory factor-5 (IRF5). Furthermore, the antifibrotic efficacy of an orally bioavailable, peripherally restricted CB_1R/iNOS hybrid inhibitor in mice with BL-PF was found to exceed that of inhibitors of either target alone, which supports the therapeutic potential of simultaneously targeting these two pathways.

Results

Increased anandamide levels in BALF from patients with IPF. Endocannabinoid levels are increased locally in certain organs and/or in the systemic circulation in disorders such as obesity, diabetes, and liver fibrosis (21, 28–30). Eventually, this results in an overactive endocannabinoid/CB_1R system that contributes to disease pathology. We analyzed human plasma and BALF from normal healthy volunteers and patients with IPF by measuring the level of the endocannabinoids, anandamide (arachidonoyl ethanolamide [AEA]) and 2-arachidonoylglycerol (2-AG). In BALF, AEA content was significantly elevated in IPF relative to normal healthy volunteers, whereas there was no change in 2-AG levels (Figure 1A). Plasma AEA and 2-AG levels were unaffected by IPF (Figure 1B). AEA levels in BALF were negatively correlated with pulmonary function in these patients (Figure 1C and Table 1).

Overexpression of CB_1R and iNOS proteins in fibrotic human lung tissue. Next, we evaluated CB_1R and iNOS protein levels by immunohistochemistry in lung tissue from patients undergoing lung transplantation and found that CB_1R and iNOS proteins were dramatically increased in IPF lungs (Figure 2A), which also exhibited marked alveolar interstitial collagen deposition (Figure 2B). The increased tissue level of AEA, coupled with the increased expression of its target CB_1R, points to an overactive endocannabinoid/CB_1R system in IPF.

Overactive endocannabinoid/CB_1R system and iNOS in mice with BL-PF. We also analyzed the endocannabinoid/CB_1R system in a bleomycin-induced murine model of PF. Lung fibrosis was histologically and biochemically evident on day 7 after oropharyngeal instillation of bleomycin, as reflected in increased collagen deposition (Figure 3A), higher Ashcroft score (Figure 3B), and higher hydroxyproline content (Figure 3C), and further progression coupled with increased mortality was evident by days 14 and 18 (Figure 3D). Gene expression of the fibrogenic markers *Tgfβ1*, *Col1a*, and *Timp1* was progressively elevated in the lungs (Figure 3E). This was coupled with significant and progressive increases in AEA, but not 2-AG, levels in both BALF and lung tissue (Figure 3, F and G), similar to the findings in human IPF (Figure 1A). Furthermore, *Cnr1* and *Nos2* mRNA were significantly increased both in lung and BALF cells at day 18 after bleomycin (Figure 3, G–I). Interestingly, at the 7-day time point, *Cnr1* mRNA was increased in BALF cells but not in lung, whereas early increase in *Nos2* mRNA was evident in lung but not in BALF cells. The progressive increase of CB_1R in the lungs of mice with BL-PF is similar to findings in human IPF, lending support to the translational relevance of this mouse model regarding the overactivity of the endocannabinoid system in PF.

The cellular levels of AEA reflect the balance between its biosynthesis and degradation, catalyzed primarily by the enzymes *N*-acyl phosphatidylethanolamine–specific phospholipase D (NAPE-PLD) and fatty acid amide hydrolase (FAAH), respectively. We found that *Napepld* expression in murine lung tissue was unchanged with bleomycin treatment at days 7 and 14 days relative to control, whereas *Faah* expression was remarkably reduced at day 7 and remained at this level at day 14 (Supplemental Figure 1; supplemental material available online with this article; https://doi.org/10.1172/jci.insight.92281DS1). This suggests that reduced FAAH activity may be one of the mechanisms by which AEA levels increase in the fibrotic lung.

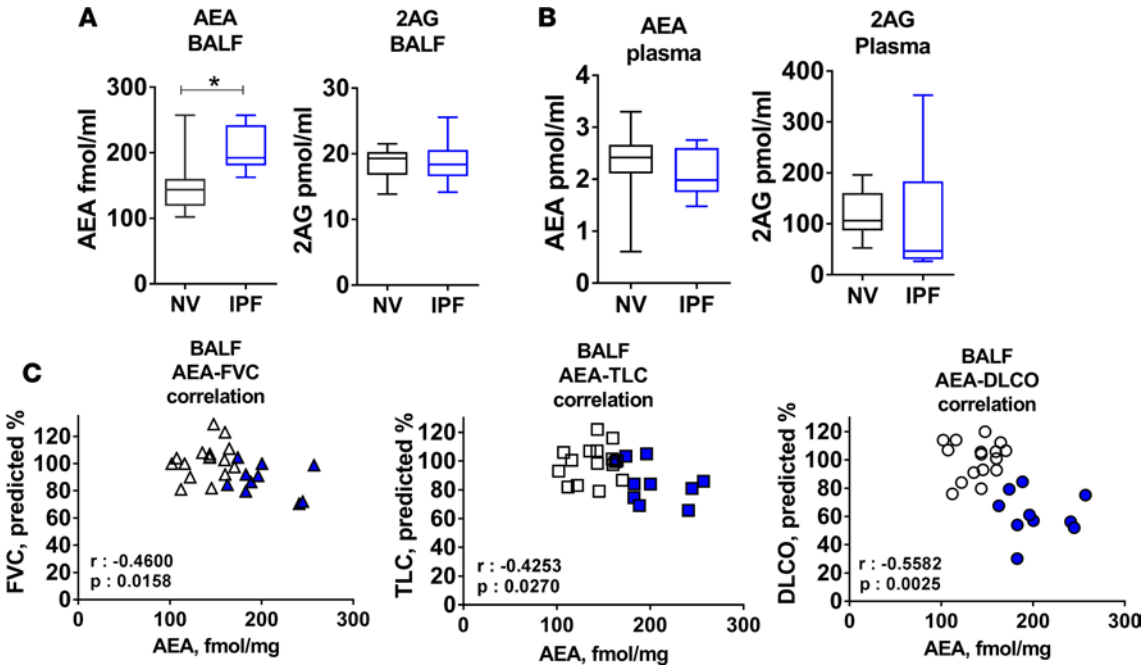

Figure 1. Negative correlation between anandamide content of BALF and pulmonary function tests in IPF patients. Anandamide (AEA) and 2-AG levels in BALF (**A**) and plasma samples (**B**) from normal volunteers (NV) and patients with idiopathic pulmonary fibrosis (IPF). Correlation with pulmonary function tests (PFT) and AEA in BALF in the same group (**C**). NV, white symbols; IPF, blue symbols. Correlation was calculated by using Pearson correlation coefficients. FVC, forced vital capacity; TLC, total lung capacity; DLCO, diffusion capacity. Data represent box-and-whisker plots; horizontal lines represent the median and 25th to 75th percentiles, and whiskers represent minimum and maximum values from 10 NV and 10 IPF subjects for plasma and 17 NV and 10 IPF subjects for BALF and PFT. Differences between the two groups were analyzed by *t* test. $^*P < 0.05$ indicates significant difference relative to NV group.

Cellular localization of CB_1R in BL-PF. In parallel with the increase in AEA levels and CB_1R gene expression, CB_1R protein levels were also elevated in lungs of BL-PF mice (Figure 4A), akin to those observed in human IPF lung tissue (Figure 2A), although the cellular localization of CB_1R is yet to be explored. Alveolar type 2 epithelial cells (ATII cells) and alveolar macrophages showed CB_1R-positive immunoreactivity in human IPF lung tissue (Figure 4B). Since ATII cells, alveolar macrophages, and myofibroblasts all have important roles in lung fibrogenesis, we attempted cell-type–specific localization of CB_1R using double immunohistochemistry and confocal microscopy. CB_1R expression by ATII cells and alveolar macrophages was indicated by their colocalization with surfactant protein C (SP-C) and CD68, respectively (Figure 4C). On the other hand, α–smooth muscle actin–positive (α-SMA–positive) lung myofibroblasts did not appear to have detectable CB_1R expression (Figure 4C).

$Cnr1^{-/-}$ and $Nos2^{-/-}$ mice display decreased fibrogenesis and improved survival relative to WT mice with BL-PF. Pharmacological inhibition or genetic deletion of *Cnr1* was reported to mitigate PF and improve survival in mice following thoracic irradiation (26), but a similar role of CB_1R in IPF and BL-PF has not yet been investigated. On the other hand, the involvement of iNOS in human IPF and in BL-PF was suggested in several prior studies (11, 15). In view of the observed activation of both the endocannabinoid/CB_1R system and iNOS in BL-PF, we explored the effect of gene deletion of *Cnr1* and *Nos2* on fibrosis development in this model. Bleomycin-induced fibrosis was diminished in both $Cnr1^{-/-}$ and $Nos2^{-/-}$ mice relative to WT mice, as determined by Masson trichrome staining (Figure 5A), Ashcroft scoring (Figure 5B), and tissue hydroxyproline content (Figure 5C). Bleomycin-induced fibroblastic activity was also attenuated in both $Cnr1^{-/-}$ and $Nos2^{-/-}$ mice, as quantified by α-SMA immunostaining (Figure 5, A and D). $Cnr1^{-/-}$ and $Nos2^{-/-}$ mice both displayed improved survival rates following bleomycin instillation (Figure 5E). The expression of the fibrogenic genes *Tgfβ1*, *Ctgf*, *Pdgfc*, *Col1a*, *Fn1*, and *Timp1* in lung tissue was also significantly reduced in both strains, relative to similarly treated WT mice (Figure 6A). Furthermore, gene expression and protein levels of the inflammatory and fibrogenic chemokines, monocyte chemotactic protein-1 (MCP-1, also known as C-C motif ligand 2 [CCL2]) and

Table 1. Human subject characteristics

	IPF (n = 10)	NV (n = 16)	P value
Age (yr)	61.4 ± 2.2	35.7 ± 2.8	<0.001
Gender (M/F)	7/3	12/4	
FEV1 (% predicted)	94.0 ± 4.1	102.1 ± 3.3	0.136
FVC (% predicted)	87.9 ± 3.7	102.3 ± 3.2	0.008
FEV1/FVC (%)	77.9 ± 1.3	78.0 ± 2.1	0.962
TLC (% predicted)	85.2 ± 4.3	100.7 ± 3.6	0.012
DLCOa (% predicted)	61.7 ± 5.0	100.4 ± 3.3	<0.001

Data represent mean ± SEM. IPF, idiopathic pulmonary fibrosis; NV, normal volunteer; M, male; F, female; FEV1, forced expiratory volume in 1 second; FVC, forced vital capacity; TLC, total lung capacity; DLCOa, diffusion capacity (adjusted).

C-X-C motif chemokine 12 (CXCL12), were significantly attenuated by the deletion of *Cnr1* but not *Nos2* (Figure 6, B and C). Bleomycin-induced *Arg1* gene expression was also attenuated by the deletion of *Cnr1* (Figure 6D).

The endocannabinoid/CB_1R system and iNOS are independently activated in BL-PF. The bleomycin-induced elevation of AEA levels was attenuated by *Cnr1* but not by *Nos2* deletion (Figure 7A), whereas the parallel increases in iNOS activity were attenuated in *Nos2*$^{-/-}$ mice but remained unaffected by *Cnr1* deletion (Figure 7B). These findings support the deleterious role of CB_1R overactivation and increased iNOS activity in lung fibrosis, while also suggesting a distinct role of these two pathways in PF pathogenesis, which justifies their combined targeting for treatment.

Deletion of Cnr1 prevents the bleomycin-induced proinflammatory and fibrogenic phenotype in alveolar macrophages. Alveolar macrophages contribute to the development of PF (31), and overactivity of macrophage CB_1R is proinflammatory (27, 28). Therefore, CB_1R expressed in alveolar macrophages may contribute to lung inflammation and fibrogenesis. Bleomycin treatment induced a progressive increase in AEA content and CB_1R expression in BAL cells (Figure 3, F and H), which paralleled the increase in fibrosis markers (Figure 3, B, C, and E). We next analyzed the immune cell population and alveolar macrophage activation in cells isolated by flow cytometry from BALF of WT, *Cnr1*$^{-/-}$, and *Nos2*$^{-/-}$ mice at 7 and 14 days after bleomycin delivery. Bleomycin-induced elevation on BAL cellularity was similar in WT mice and mice lacking either the *Cnr1* or *Nos2* genes (Supplemental Figure 2A). Additionally, bleomycin-induced increases in the levels of $CD11c^+$ alveolar macrophages and infiltrated $GR1^+$ neutrophils, $CD4^+$ T lymphocytes, $CD19^+$ B lymphocytes, and NK1.1 cells were similar in the three mouse strains (Supplemental Figure 2, B–D, and Supplemental Figure 3). $CD11c^+$ alveolar macrophages were further sorted into $CD11b^+$ proinflammatory and $CD206^+$ profibrotic cells. The bleomycin-induced increase in $CD11b^+$ cell number and expression intensity was evident already after 7 days, whereas these increases were delayed and only appeared after 14 days in the case of $CD206^+$ cells (Figure 8). Furthermore, deletion of *Cnr1*, but not *Nos2*, blunted the increase in both the abundance and the intensity of cell surface expression of the respective antigens in these two cell types (Figure 8).

Combined CB_1R/iNOS inhibition has superior antifibrotic efficacy in BL-PF over CB_1R inhibition alone.

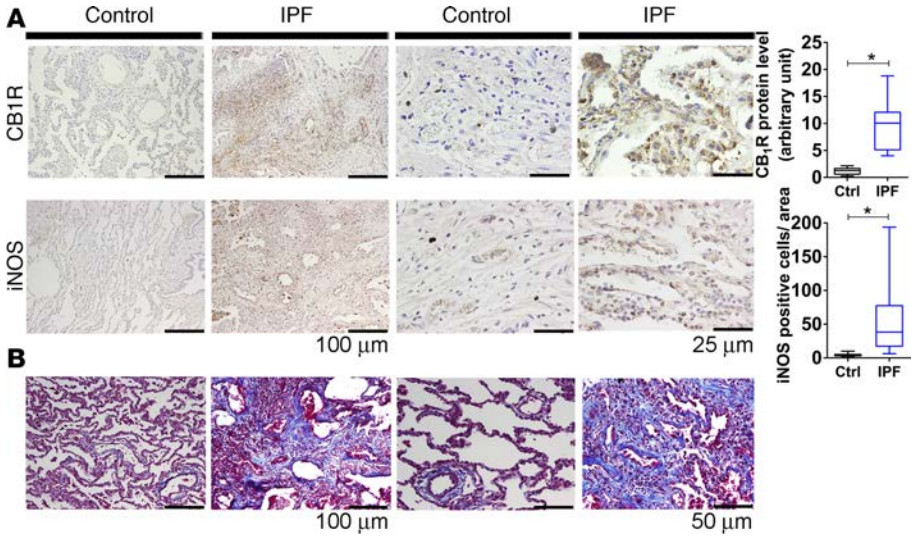

Figure 2. Increased CB_1R and iNOS protein in lung samples from IPF patients. CB_1R and iNOS immunohistochemistry in human lung tissue sections from idiopathic pulmonary fibrosis (IPF) patients and controls without fibrotic lung disease (**A**). Fibrosis visualized by Masson trichrome–stained sections from the same subjects (**B**). Data represent box-and-whisker plots; horizontal lines represent the median and 25th to 75th percentiles, and whiskers represent minimum and maximum values from 5 normal volunteers or 10 IPF subjects. Data were analyzed by *t* test. *P < 0.05 indicates significant difference relative to control group. Scale bar: 25 μm (**A**, right columns); 50 μm (**B**, right columns); 100 μm (**A** and **B**, left columns).

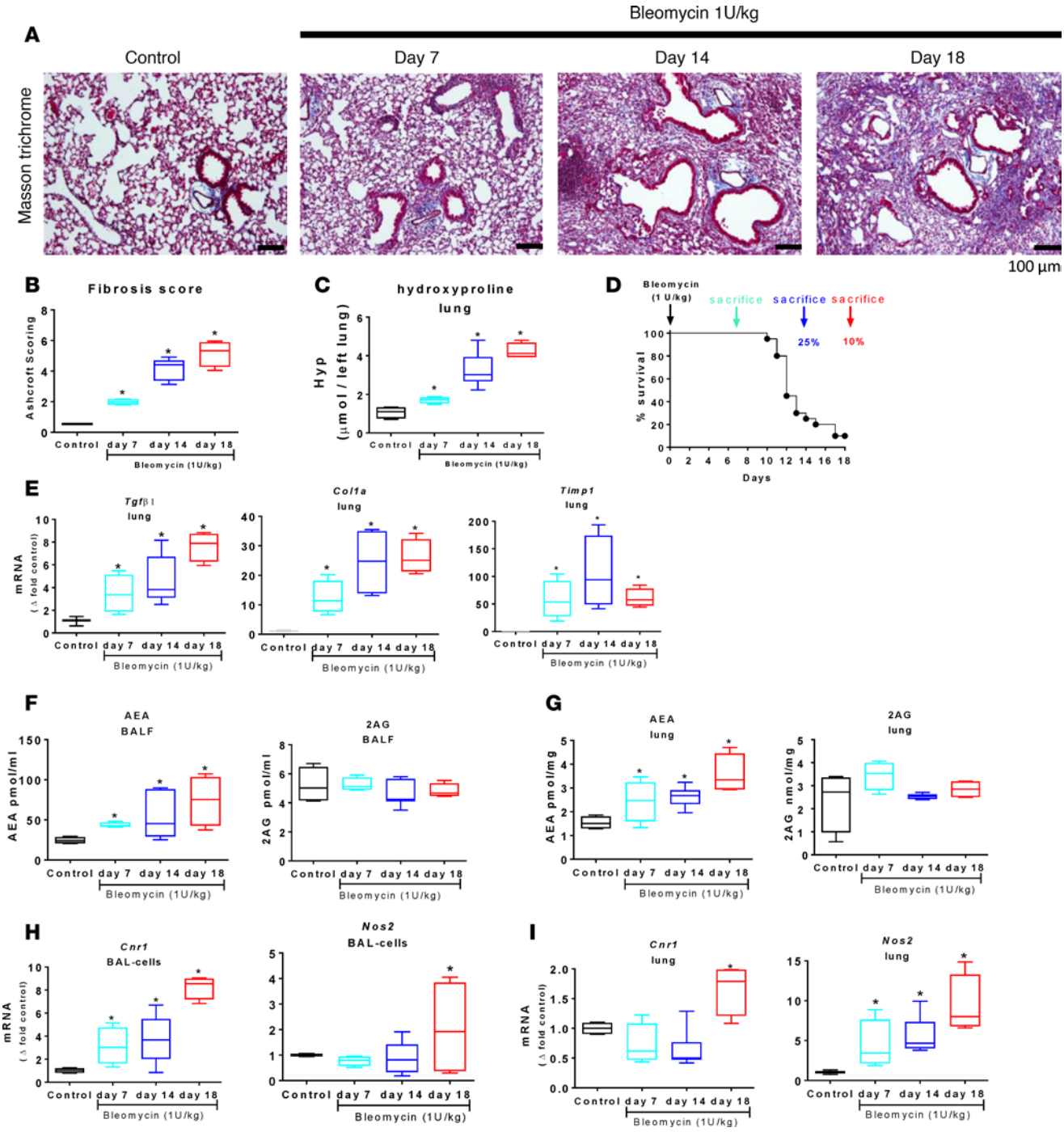

Figure 3. Increased tissue levels of anandamide, CB_1R, and iNOS during progression of bleomycin-induced fibrosis in mice. Masson trichrome staining (**A**), fibrosis grade assessed by Ashcroft scoring (**B**) or by lung hydroxyproline content (**C**), and survival curve (**D**). Gene expression of fibrosis markers *Tgfβ1*, collagen 1a (*Col1a*), and tissue inhibitor of metalloproteinase-1 (*Timp1*) (**E**). Endocannabinoid levels in BALF (**F**) and lung (**G**). Gene expression of *Cnr1* and *Nos2* in BALF cells (**H**) and lung (**I**). Data represent box-and-whisker plots; horizontal lines represent the median and 25th to 75th percentiles, and whiskers represent minimum and maximum values from 4 (control), 5 (day 7), 10 (day 14), and 4 mice (day 18). Data were analyzed by 1-way ANOVA followed by Dunnett's multiple comparisons test. $^*P < 0.05$ indicates significant difference from control group. Scale bar: 100 μm.

We developed MRI-1867 as a dual-target peripheral CB_1R/iNOS inhibitor and demonstrated its superior efficacy in rodent models of liver fibrosis relative to inhibition of CB_1R or iNOS alone (21). MRI-1867 and rimonabant are equipotent in antagonizing CB_1R. We selected an oral dose of 10 mg/kg for rimonabant and MRI-1867 and an intraperitoneal dose of 10 mg/kg for AM6545, because this dose

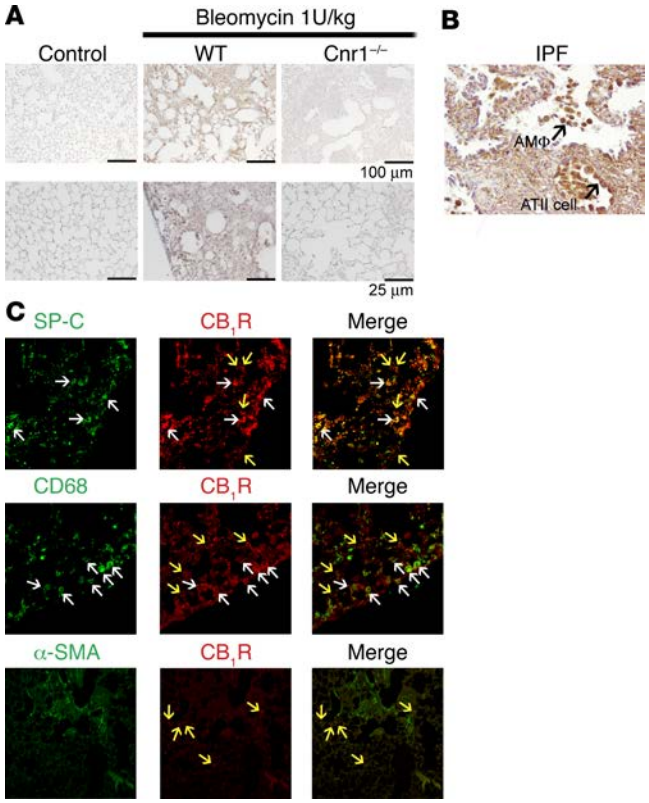

Figure 4. Cellular localization of CB_1Rs after bleomycin induction in fibrotic mouse lung. CB_1R immunohistochemistry in mouse lung tissue sections from WT control, WT BL-PF, and *Cnr1*$^{-/-}$ BL-PF at 14 days after bleomycin challenge (**A**). CB_1R immunohistochemistry in human idiopathic pulmonary fibrosis (IPF) lung tissue, showing CB_1R expression in alveolar macrophages (AMΦ) and alveolar epithelial type 2 (ATII) cells. Original magnification: ×40 (**B**). CB_1R/SP-C, CB_1R/CD68, and CB_1R/α-SMA double immunohistochemistry and imaging by confocal microscopy in lung tissue from WT BL-PF mice. Colocalization marked by white arrows, with distinct localization marked in yellow. Original magnification, ×40 (**C**). Scale bar: 25 μm (**A**, bottom row); 100 μm (**A**, top row).

causes near-maximal antagonism of the CB_1R agonist–induced decrease in upper GI motility (21). Following oral administration of 10 mg/kg MRI-1867, the peak concentration measured in lung tissue (~20 μM, Supplemental Figure 4A) was well above concentrations that inhibit iNOS activity, as determined in LPS-injected mouse lung homogenates (Supplemental Figure 4B). In contrast, rimonabant at concentrations of up to 10 μM did not inhibit iNOS activity in the same in vitro assay (Supplemental Figure 4B). The peripherally restricted CB_1R antagonist AM6545 was pharmacologically characterized earlier (32), and its antifibrotic efficacy was recently shown on prevention of radiation-induced PF (26). We next compared the antifibrotic efficacy of MRI-1867, rimonabant, and AM6546 by chronic administration of a 10 mg/kg daily oral dose for rimonabant and MRI-1867 or intraperitoneal dose for AM6545 to mice with bleomycin-induced fibrosis. Treatment was started either immediately following bleomycin administration for rimonabant and MRI-1867 (to assess their ability to prevent fibrosis development) or 7 days after bleomycin instillation for rimonabant, MRI-1867, and AM6545 (to assess slow down or progression arrest of PF), as illustrated in Figure 9, A and B, respectively.

In the prevention paradigm, MRI-1867 and rimonabant yielded survival rates of 92% and 80%, respectively, both of which were significantly higher than the 36% survival rate in the vehicle group (Figure 9A). Similarly, both MRI-1867 and rimonabant significantly reduced fibrosis development, as quantified by hydroxyproline content (Figure 9C).

In the fibrosis progression arrest paradigm, only MRI-1867 caused a significant increase in survival rate (100% with MRI-1867 compared with 36% in the vehicle group), whereas the 70% and 71% survival rates in the rimonabant and AM6545 groups were not significantly different from that of the vehicle group (Figure 9B).

In the progression arrest paradigm, only MRI-1867, and not the single target CB_1R antagonists, was able to significantly attenuate fibrosis compared with the vehicle group, as indicated by the reduction of lung hydroxyproline content (Figure 9C), which implies the role of iNOS inhibition in this effect.

Similarly, MRI-1867 was significantly more efficacious than rimonabant in attenuating the expression of the fibrogenic genes *Ctgf*, *Pdgfc*, *Timp1*, *Col1a*, and *Fn1*, although their efficacy was comparable in reducing *Tgfb1* expression (Figure 10A). The bleomycin-induced increase in iNOS activity was unaffected by rimonabant but completely abrogated by MRI-1867 (Figure 10B), which mirrored the similar effect of *Nos2* deletion but not *Cnr1* deletion (Figure 7). On the other hand, the bleomycin-induced

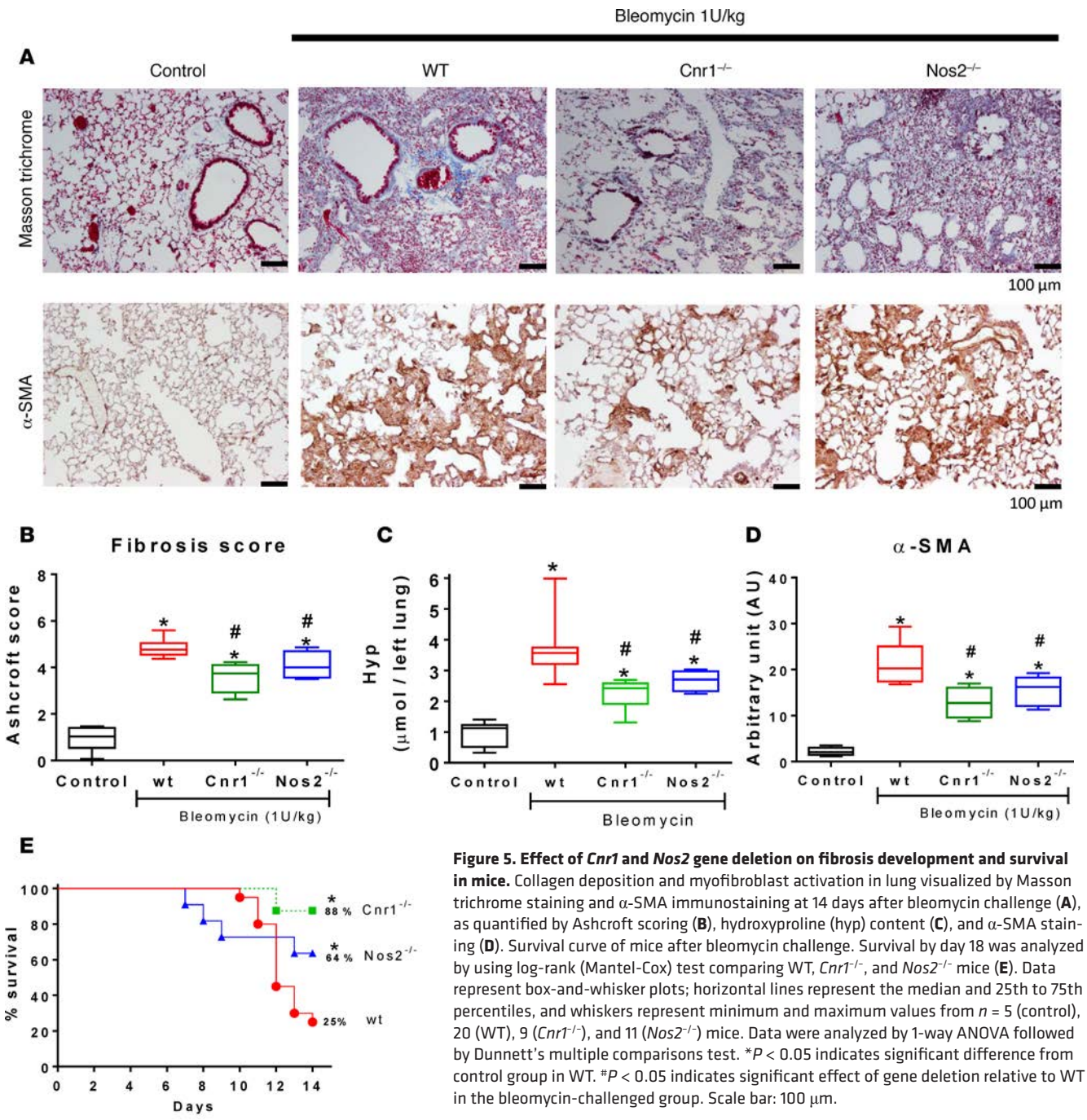

Figure 5. Effect of *Cnr1* and *Nos2* gene deletion on fibrosis development and survival in mice. Collagen deposition and myofibroblast activation in lung visualized by Masson trichrome staining and α-SMA immunostaining at 14 days after bleomycin challenge (**A**), as quantified by Ashcroft scoring (**B**), hydroxyproline (hyp) content (**C**), and α-SMA staining (**D**). Survival curve of mice after bleomycin challenge. Survival by day 18 was analyzed by using log-rank (Mantel-Cox) test comparing WT, *Cnr1*$^{-/-}$, and *Nos2*$^{-/-}$ mice (**E**). Data represent box-and-whisker plots; horizontal lines represent the median and 25th to 75th percentiles, and whiskers represent minimum and maximum values from $n = 5$ (control), 20 (WT), 9 (*Cnr1*$^{-/-}$), and 11 (*Nos2*$^{-/-}$) mice. Data were analyzed by 1-way ANOVA followed by Dunnett's multiple comparisons test. *$P < 0.05$ indicates significant difference from control group in WT. #$P < 0.05$ indicates significant effect of gene deletion relative to WT in the bleomycin-challenged group. Scale bar: 100 μm.

increase in AEA levels was completely abolished by either rimonabant or MRI-1867, reflecting the role of CB_1R blockade (Figure 10C).

We also tested partial CB_1R antagonism using a dose of 3 mg/kg/d for both rimonabant and MRI-1867 in both the fibrosis prevention and the progression arrest paradigms (Supplemental Figure 5). As expected, survival rates were lower than for the 10 mg/kg/d doses (Figure 9) but were qualitatively similar. As before, only MRI-1867, and not rimonabant, caused a significant increase in survival rate in the progression arrest paradigm (Supplemental Figure 5). These data confirm the deleterious role of the two targets in PF and support the rationale of their joint targeting for treatment.

CB_1R-induced IRF5 expression in lung during PF. IRF5, a cytokine that promotes the proinflammatory polarization of macrophages, has recently been implicated in both hepatic and skin fibrosis (33, 34), as well as in β cell loss in type 2 diabetes, the latter being in part mediated by CB_1R activation of proinflammatory macrophages

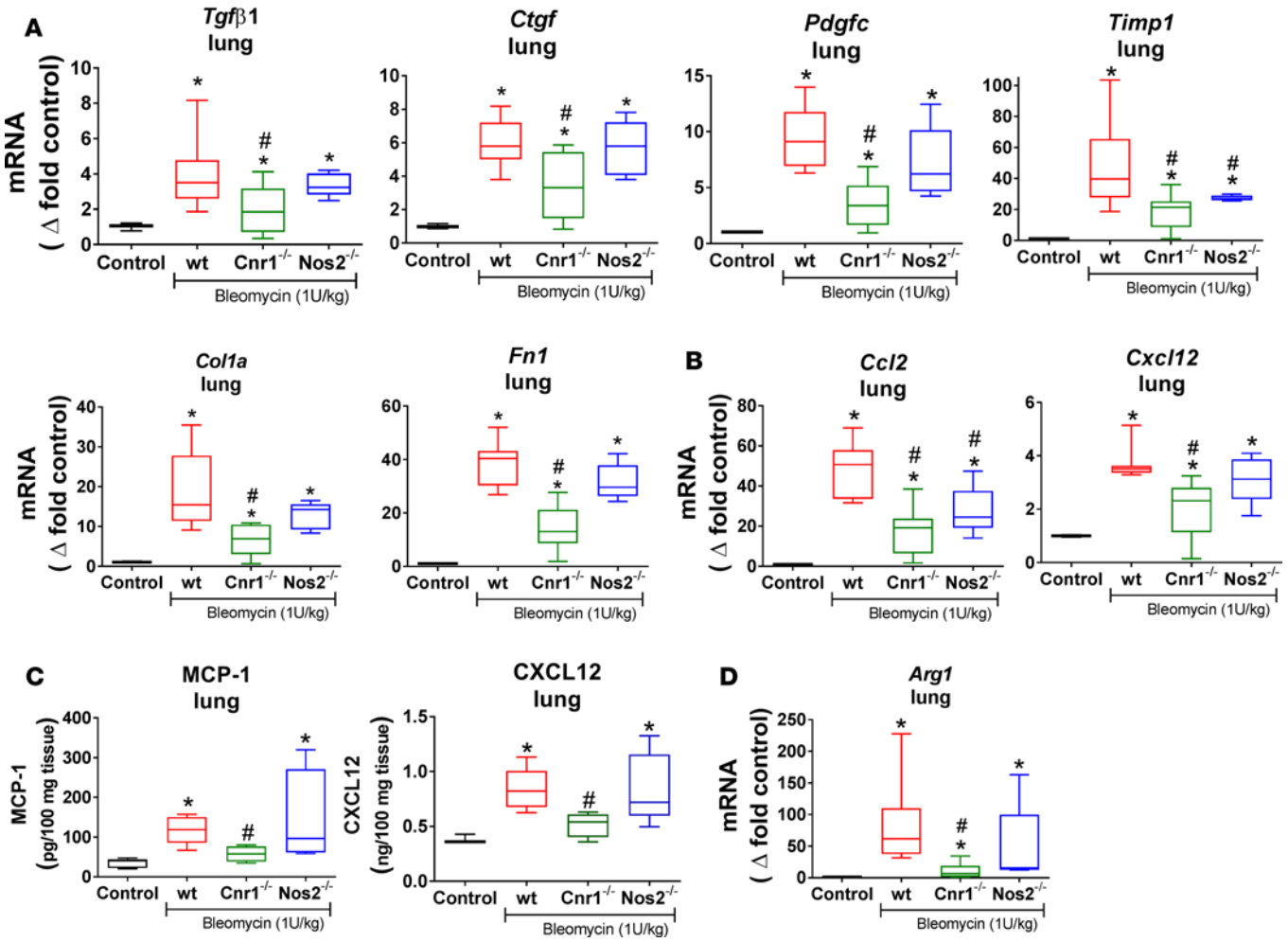

Figure 6. Effect of *Cnr1* and *Nos2* gene deletion on the expression in the lung of fibrogenic markers. *Tgfβ1*, connective tissue growth factor (C*tgf*), platelet-derived growth factor c (*Pdgfc*), collagen 1a (*Col1a*), fibronectin 1 (*Fn1*), and tissue inhibitor of metalloproteinase-1 (*Timp1*) (**A**). Chemokine C-C motif ligand 2 (*Ccl2*) and C-X-X motif chemokine 12 (*Cxcl12*) (**B**). Protein levels of MCP-1 and CXCL12 (**C**) and gene expression of arginase 1 (*Arg1*) (**D**) in lung tissue at 14 days after bleomycin challenge from control mice and bleomycin-treated WT, *Cnr1*$^{-/-}$, and *Nos2*$^{-/-}$ mice. Data represent box-and-whisker plots; horizontal lines represent the median and 25th to 75th percentiles, and whiskers represent minimum and maximum values from n = 5 (control), 20 (WT), 9 (*Cnr1*$^{-/-}$), and 11 (*Nos2*$^{-/-}$) mice. Data were analyzed by 1-way ANOVA followed by Dunnett's multiple comparisons test. *P < 0.05 indicates significant difference from control group. $^{\#}P$ < 0.05 indicates significant effect of gene deletion relative to WT in the bleomycin-challenged group.

(28). Because we observed that CB_1R activation is proinflammatory and profibrotic in alveolar macrophages, we investigated the regulation of *Irf5* expression by CB_1R in lung tissue during PF. Bleomycin treatment induced *Irf5* expression, which was attenuated either by genetic deletion or pharmacological inhibition of CB_1R but not by deletion of *Nos2* (Figure 11, A and B). A similar pattern of changes was noted in the IL1β tissue levels in the lung (Figure 11C), which is compatible with our earlier findings that IRF5 mediates CB_1R-induced IL1β secretion in proinflammatory macrophages (28).

Discussion

Here, we report, for the first time to our knowledge, a robust upregulation of both CB_1R and one of its endogenous ligands, AEA, in lung and BALF samples from patients with IPF and from mice with BL-PF, suggesting a pathogenic role of the endocannabinoid/CB_1R system in IPF. This was strongly supported by the findings that *Cnr1*$^{-/-}$ deletion in mice reduced bleomycin-induced fibrosis, improved survival (Figures 5 and 6), and reduced the activation of alveolar macrophages (Figure 8), suggesting that pulmonary CB_1R is both profibrogenic and proinflammatory in BL-PF.

The expression of the proinflammatory enzyme iNOS was also induced in both human IPF and in

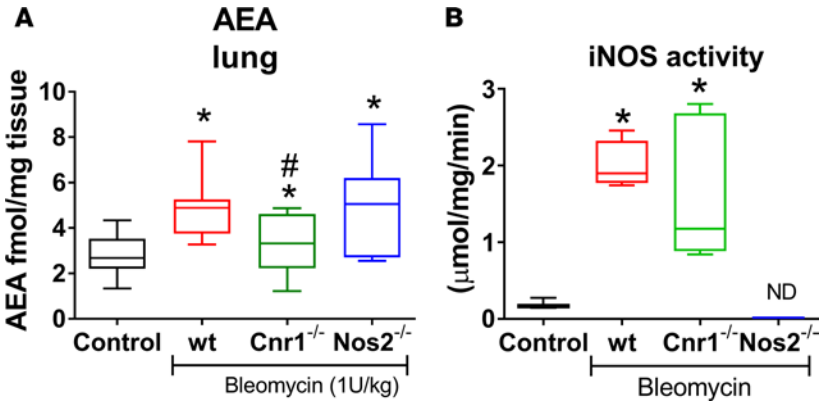

Figure 7. Distinct pattern of activation of iNOS and AEA in pulmonary fibrosis. AEA levels (**A**) and iNOS enzyme activity (**B**) in lung tissue at 14 days after bleomycin challenge from control mice and bleomycin-treated WT, *Cnr1*$^{-/-}$, and *Nos2*$^{-/-}$ mice. Data represent box-and-whisker plots; horizontal lines represent the median and 25th to 75th percentiles, and whiskers represent minimum and maximum values from n = 5 (control), 20 (WT), 9 (*Cnr1*$^{-/-}$), and 11 (*Nos2*$^{-/-}$) mice. Data were analyzed by 1-way ANOVA followed by Dunnett's multiple comparisons test. *P < 0.05 indicates significant difference from control group. $^{\#}P$ < 0.05 indicates significant effect of gene deletion relative to WT in the bleomycin-challenged group.

mice with BL-PF, and *Nos2* deletion similarly provided partial protection from BL-PF. These findings identify both CB_1R and iNOS in lung tissue as therapeutic targets in PF. Most importantly, we tested the therapeutic strategy of simultaneously inhibiting these two proteins with a single chemical entity, resulting in significantly greater attenuation of fibrosis progression and improvement in survival rate compared with equivalent antagonism of CB_1R alone. This was most evident in a paradigm testing the arrest of progression of established bleomycin-induced fibrosis, in which treatment with the hybrid CB_1R/iNOS inhibitor completely arrested fibrosis progression and dramatically improved the survival rate from 25% to 100%, making the current findings clinically more relevant.

Injury of lung epithelial cells is considered critical for the initiation of the fibrotic process. In addition, immune cells have an important role in alveolar inflammation and progression to PF. Therefore, multicellular interactions in the lung constitute the fibrogenic environment and affect progression of the disease. In the lung, CB_1R is expressed in different cell populations, including ATII cells (35), bronchial epithelial cells (36), and both resident and infiltrating alveolar macrophages (37). We found a high degree of colocalization of CB_1R with the ATII cell marker SP-C (Figure 4B). ATII cells play an important role in recruiting fibrocytes (38) and promoting fibroblast proliferation in IPF (39) by producing fibrocyte-recruiting chemokines such as MCP-1 and CXCL12 (40, 41) and fibrogenic growth factors such as CTGF (42). In fact, fibrocyte recruitment is considered an indicator of poor prognosis in IPF (43). Bleomycin induced significantly greater increases in *Ccl2* and *Cxcl12* gene expression in WT mice than in *Cnr1*$^{-/-}$ mice (Figure 6B), and protein levels of MCP-1 and CXCL12 in lung were also dramatically attenuated in *Cnr1*$^{-/-}$ mice (Figure 6C), which implicates endocannabinoids acting via CB_1R in promoting chemokine secretion. Furthermore, a recent study exemplified an interaction between ATII cells and alveolar macrophages in fibrogenesis: MCP-1 secretion is increased in ATII cells from mice with Hermansky-Pudlak lung fibrosis, which increases alveolar macrophages in the lung, resulting in increased TGF-β secretion (44). In the current study, bleomycin-induced *Tgfb1* gene expression was attenuated both in *Cnr1*$^{-/-}$ mice and following CB_1R antagonist treatment. This suggests that activation of CB_1R in ATII cells may be one of the cell-type–specific mechanisms in the pathogenesis of PF. This intriguing possibility remains to be further explored.

We found that CB_1R and AEA are present in cells isolated from BALF and that their expression is strongly increased following bleomycin administration (Figure 3, F and H). Interestingly, *Cnr1* mRNA in BALF cells and AEA levels in BALF were already highly elevated during the early inflammatory phase at day 7 of bleomycin treatment and increased further during the fibrogenic phase from day 14 to 18 (Figure 3, F and H). BALF cells constitute a mixed population of immune cells, and future studies will aim to explore cell-type–specific changes in endocannabinoids and their receptors in this cell population. In contrast to the time course observed in BAL cells, *Cnr1* expression in the lung specimens remained unchanged at days 7 and 14 and only increased by day 18 following bleomycin treatment (Figure 3I). This is compatible with the notion that an early increase in endocannabinoid tone in proinflammatory cells triggers similar changes in lung tissue, which then promotes the later stages of fibrogenesis. The late increase in CB_1R expression in the lungs of BL-PF mice parallels the robust increase in CB_1R protein levels in the lungs of patients with severe IPF who subsequently had lung transplantation (Figure 2A).

We also analyzed the influence of CB_1R and iNOS activity on the activation of alveolar macrophages present in BALF. Alveolar macrophages are detectable as a $CD68^{dim}F4/80^{dim}CD11c^{+}$ cell popu-

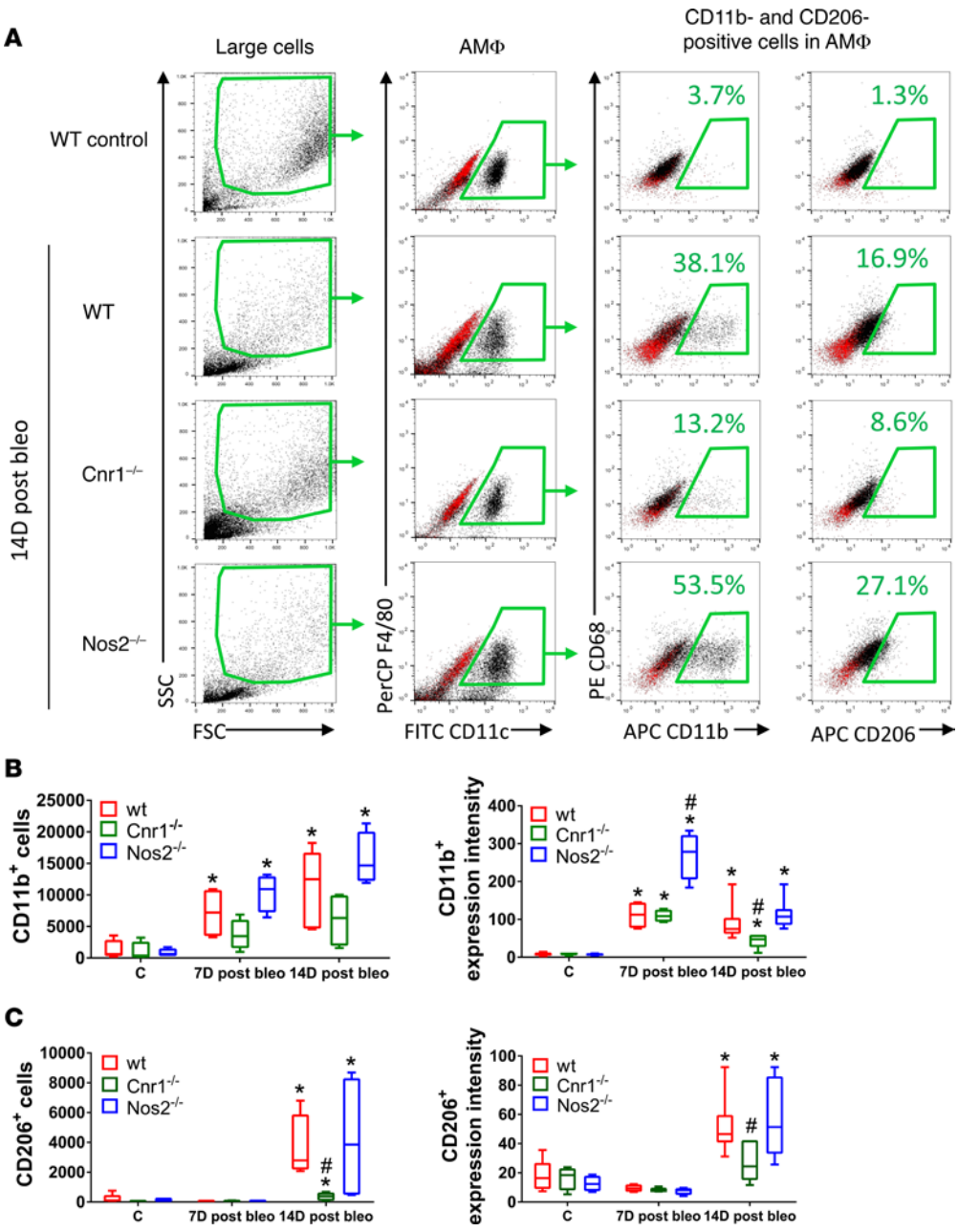

Figure 8. Effect of *Cnr1* and *Nos2* gene deletion on alveolar macrophage activation status for CD11b and CD206 expression. Gating strategy in flow cytometry experiment, with representative histograms for defining CD11b$^+$ and CD206$^+$ cells in the alveolar macrophage (AMΦ) population using BAL cells from WT, *Cnr1*$^{-/-}$, and *Nos2*$^{-/-}$ mice from either the control group or mice after 14-day bleomycin treatment (14D post bleo) (**A**). CD11b$^+$ and CD206$^+$ cells were defined by gating to exclude >99.5% of unstained, autofluorescent cells. Unstained cells are shown as red dots. Cell number and surface expression intensity of CD11b$^+$ cells (**B**) and CD206$^+$ cells (**C**), isolated from control mice, after 7-day bleomycin treatment (7D post bleo) or after 14-day bleomycin treatment (14D post bleo). Data represent box-and-whisker plots; horizontal lines represent the median and 25th to 75th percentiles, and whiskers represent minimum and maximum values from n = 6 (WT), 4 (*Cnr1*$^{-/-}$), and 5 (*Nos2*$^{-/-}$) mice. $^*P < 0.05$ indicates significant difference from corresponding control group. $^{\#}P < 0.05$ indicates significant difference from values in WT mice within the same treatment group (2-way ANOVA followed by multiple comparisons test).

lation in BALF, which is distinct from the phenotype of other tissue macrophages. This alveolar macrophage population usually does not express the M1 marker CD11b but expresses CD206 (macrophage mannose receptor). Nonetheless, it is known that during fibrogenesis alveolar macrophages acquire a proinflammatory and profibrotic phenotype, which is characterized by elevated expression of both CD11b and CD206 (45, 46). There is evidence for increased expression of CD206$^+$ macrophages in alveolar macrophages isolated from patients with IPF versus controls, which is compatible with the fibrogenic role of this subset of alveolar macrophages (47). In the present study, bleomycin treatment induced a selective increase in both the number of CD11b$^+$ cells and the cell surface expression of CD11b within 7 days, whereas similar changes in CD206$^+$ cells only appeared 14 days after bleomycin treatment (Figure 8, B and C). These data suggest that CD11b$^+$ alveolar macrophages contribute the proinflammatory milieu that promotes fibrosis initiation at day 7, at which time the number of CD206$^+$ macrophages was still low (Figure 3, A–C, and Figure 8, B and C). On the other hand, a late

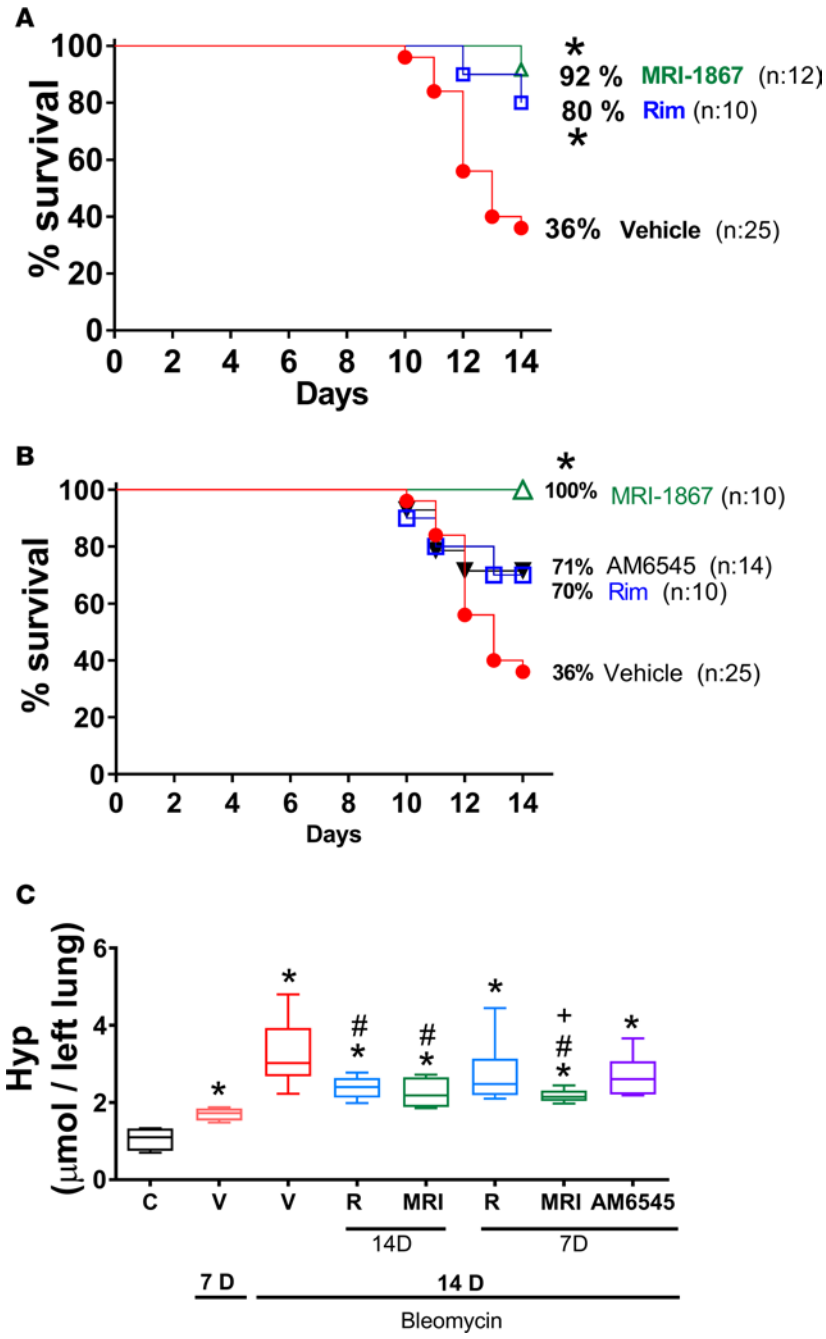

Figure 9. Effects of rimonabant, MRI-1867, or AM6545 treatment on survival and lung fibrosis development in bleomycin-treated mice. Survival curves for the fibrosis prevention (**A**) and regression (**B**) treatment paradigms in bleomycin-instilled mice following chronic treatment with vehicle, rimonabant (Rim), MRI-1867, both rimonabant and MRI-1867 at 10 mg/kg, PO, or AM6545 at 10 mg/kg, intraperitoneally. Survival was analyzed by using log-rank (Mantel-Cox) test. **P* < 0.05 indicates significant difference from bleomycin-treated vehicle group. Hydroxyproline levels in lung (**C**). Data represent box-and-whisker plots; horizontal lines represent the median and 25th to 75th percentiles, and whiskers represent minimum and maximum values from 4 mice (control and Post-bleo 7D vehicle) and 10–25 mice for other groups, as indicated in the figure. The length of vehicle treatment (starting at day 0 or 7) did not significantly affect survival; therefore, these data were merged and used as control for both treatment paradigms, as shown in **A** and **B**. Data were analyzed by 1-way ANOVA followed by Dunnett's multiple comparisons test. **P* < 0.05 indicates significant difference from control group. #*P* < 0.05 indicates significant difference from the vehicle group 14 days after bleomycin. +*P* < 0.05 indicates significant difference from the rimonabant-treated group. Hyp, hydroxyproline; C, control; V, vehicle; R, rimonabant; MRI, MRI-1867.

rise in fibrogenic CD206$^+$ alveolar macrophages at day 14 could support their role in fibrosis progression. Interestingly, *Cnr1*$^{-/-}$ deletion moderated the bleomycin-induced increase in both CD11b and CD206 expression compared with cells from similarly treated WT mice (Figure 8). Although both CB_1R and iNOS are expressed in alveolar macrophages, only CB_1R is involved in activating alveolar macrophages, which reflects the distinct roles of these two targets in PF pathogenesis. This further supports the dual, proinflammatory and profibrogenic, function of CB_1R in alveolar macrophages. CB_1R, possibly on ATII cells, also promotes the secretion of chemokines involved in macrophage activation, as discussed above (Figure 6). The multicellular fibrogenic mechanisms modulated by CB_1R in the lung are schematically illustrated in Figure 12.

There are multiple myeloid cell subsets in the lung, such as alveolar macrophages, interstitial macrophages, lung monocytes, and blood monocytes (48). We found colocalization of CB_1R with the macrophage marker CD68 in the lung (Figure 4B). However, flow cytometry analyses using BALF cells limited our observations to the alveolar macrophage subpopulation. Considering the proinflammatory function of CB_1R in macrophages (27), further studies are warranted to explore the role of CB_1R in other macrophage subsets in PF.

Macrophages in the lung play an important role in regulating inflammation, injury, and fibrosis (49). IRF5 has emerged as a master regulator of the proinflammatory polarization of macrophages (50) and has also been implicated in promoting acute and chronic inflammatory conditions in the lung (51). Furthermore, IRF5 is overactivated in bleomycin-induced skin and lung fibrogenesis, whereas genetic deletion of IRF5 mitigates these conditions (34). IRF5 is also involved in the activation of liver macrophages during liver fibrosis in mice and human subjects, and its expression positively correlated with clinical markers of liver damage, whereas deletion of IRF5 in myeloid cells protects the liver from fibrogenesis (33). Together, these findings

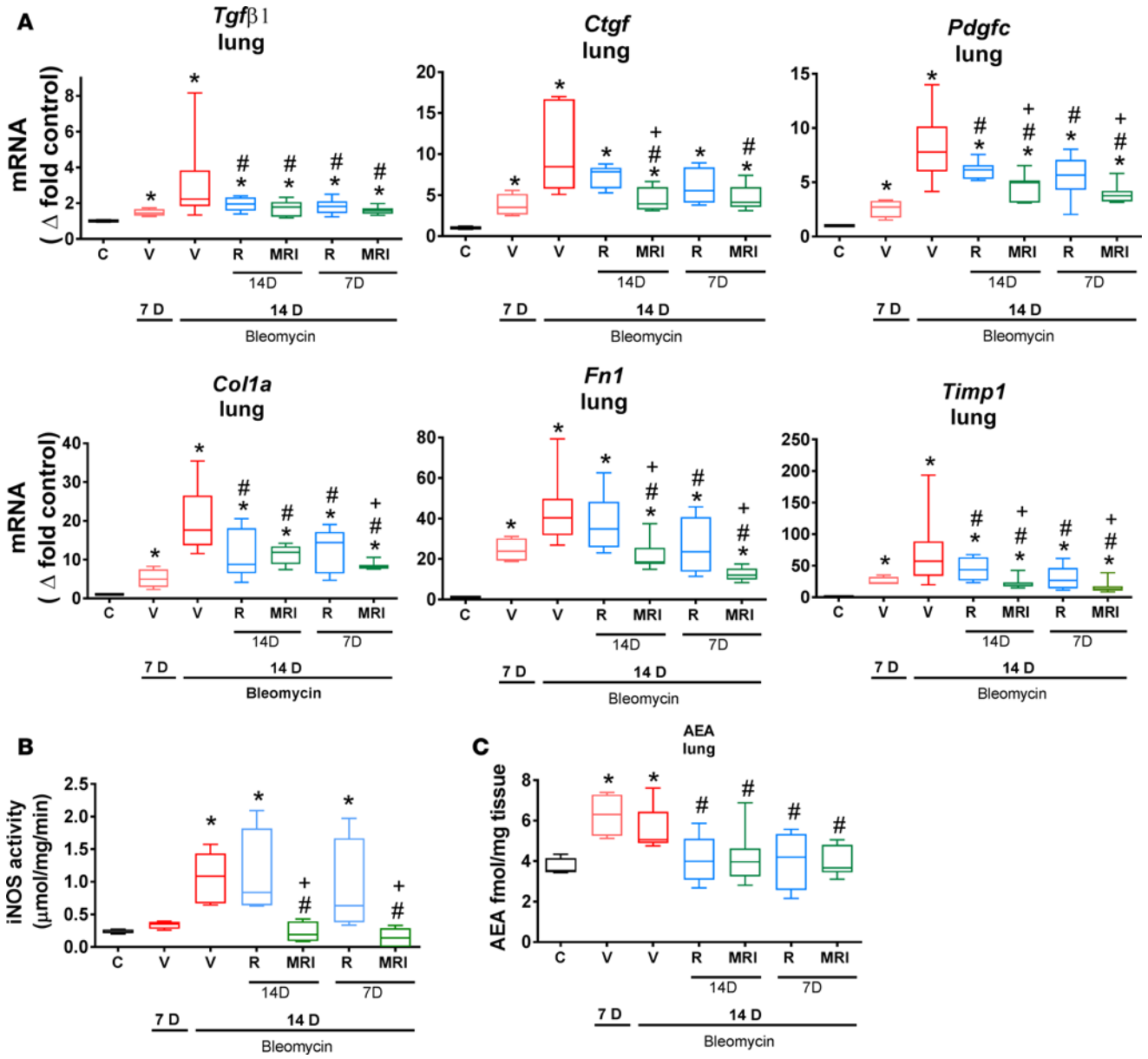

Figure 10. Effect of CB_1R blockade (with rimonabant) or CB_1R/iNOS dual inhibition (with MRI-1867) on gene expression profiles of fibrosis in WT mice following treatment from day 1–14 or day 7–14 after bleomycin treatment with vehicle, rimonabant, or MRI-1867 (10 mg/kg, PO). Gene expression of fibrogenic markers *Tgfβ1*, *Ctgf*, *Pdgfc*, *Col1a*, *Fn1*, and *Timp1* (**A**). iNOS activity in lung (**B**). Level of AEA in lung (**C**). Data represent box-and-whisker plots; horizontal lines represent the median and 25th to 75th percentiles, and whiskers represent minimum and maximum values from 4–9 mice per group. Data were analyzed by 1-way ANOVA followed by Dunnett's multiple comparisons test. *$P < 0.05$ indicates significant difference from control group. #$P < 0.05$ indicates significant difference from 14D vehicle group. +$P < 0.05$ indicates significant difference from the rimonabant-treated group. C, control; V, vehicle; R, rimonabant; MRI, MRI-1867; 7D, treatment from day 7–14; 14D, treatment from day 1–14.

highlight the essential role of IRF5 in fibrogenesis, as a regulator of macrophage activation. We recently reported that IRF5 is an obligatory mediator of CB_1R-induced β cell loss by promoting the secretion of the cytotoxic cytokines TNF-α and IL1β in macrophages infiltrating the pancreatic islets (28). In the current study, bleomycin treatment induced *Irf5* expression and IL1β protein levels in the lung, both of which were abrogated either by deletion or pharmacological antagonism of CB_1R (Figure 11), supporting the role of IRF5 as a downstream mediator of the proinflammatory effect of CB_1R activation in the fibrotic lung.

The question arises as to what mechanism(s) trigger the increased endocannabinoid/CB_1R signaling, which then contributes to lung fibrogenesis. The observed selective increase in AEA, but not 2-AG, levels in the fibrotic lungs of both mice and patients with IPF suggests the involvement of biosynthetic

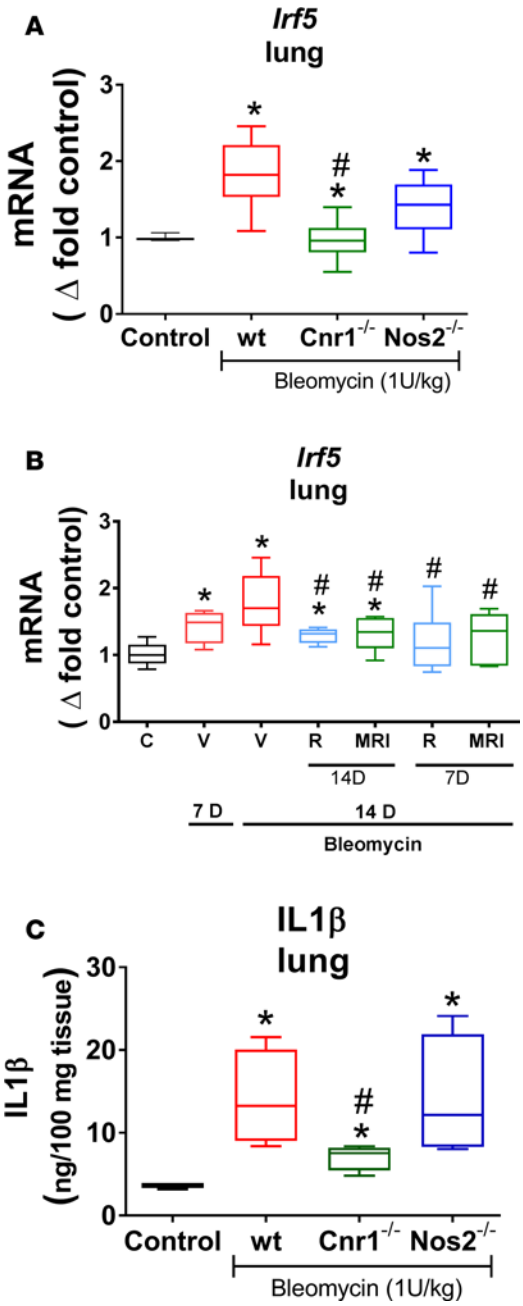

Figure 11. Effect of *Cnr1* and *Nos2* gene deletion or pharmacological inhibition on *Irf5* expression in the lung. *Irf5* expression in lung tissue from control mice (n = 5) 14 days after bleomycin treatment in WT (n = 20), *Cnr1*$^{-/-}$ (n = 9), and *Nos2*$^{-/-}$ mice (n = 11) (**A**). *Irf5* expression in bleomycin-challenged WT mice treated from day 1–14 (14D) or day 7–14 (7D) with vehicle (V), rimonabant (R), MRI-1867 (MRI), or both rimonabant and MRI-1867 at 10 mg/kg, PO. Data from n = 5 (control), 5 (V, 7D), 12 (V, 14D), and 8 mice (rimonabant and MRI-1867 treatments groups) are shown (**B**). C, control. IL1β protein levels in lung tissue lysates from control mice (n = 4) 14 days after bleomycin treatment in WT (n = 6), *Cnr1*$^{-/-}$ (n = 5), and *Nos2*$^{-/-}$ mice (n = 5) (**C**). Data represent box-and-whisker plots; horizontal lines represent the median and 25th to 75th percentiles, and whiskers represent minimum and maximum values, and were analyzed by 1-way ANOVA followed by Dunnett's multiple comparisons test. $^{*}P < 0.05$ indicates significant difference from control group. $^{\#}P < 0.05$ indicates significant effect of either gene deletion or pharmacological inhibition relative to WT vehicle in the bleomycin-challenged group.

and/or degradative pathways unique to AEA, as reported earlier in response to various proinflammatory stimuli (52, 53). We found that the gene expression of FAAH, the enzyme responsible for the in vivo metabolism of AEA, was downregulated in the mouse lung as early as day 7 after bleomycin treatment and remained low during the fibrogenic phase, whereas gene expression of the AEA biosynthetic enzyme NAPE-PLD remained unchanged (Supplemental Figure 1). Thus, reduced enzymatic degradation of AEA likely accounts for the parallel increase in its tissue levels by day 7 and its subsequent plateau (Figure 10C). Indeed, a similar decrease in FAAH expression as well as activity in fibroblasts has been documented in experimental systemic sclerosis, which was exacerbated by genetic deletion or pharmacological inhibition of FAAH (54).

Multiple cell types, including infiltrating immune cells, are believed to contribute to inflammation and fibrogenesis in PF, and macrophages, dendritic cells and lymphocytes have all been found to have elevated levels of AEA in response to inflammatory stimuli (52, 53, 55, 56). On the other hand, human lung macrophages isolated from lungs adenocarcinoma patients, which display M2-like polarization, do not contain elevated levels of AEA following in vitro exposure to LPS (37). In addition, pulmonary inflammation induced by aerosolized LPS, which is not associated with significant cell damage, exhibited neutrophil infiltration and secretion of inflammatory cytokines but no increase in AEA in BALF (57). These latter findings suggest that acute inflammation alone may be insufficient to trigger an increase in AEA in BALF cells, which may require additional injury to interstitial cells and probably chronic epithelial cell injury.

As for the parallel upregulation of CB_1R in the fibrotic lung, this may be secondary to the increase in AEA levels. There is published evidence for "autoinduction" of CB_1R expression, whereby endocannabinoid activation of CB_1R induces CB_1R gene expression in various cell-types, including T lymphocytes (58) and hepatocytes (59), and, conversely, chronic CB_1R blockade reverses the upregulation of hepatic CB_1R in mice with diet-induced obesity (60).

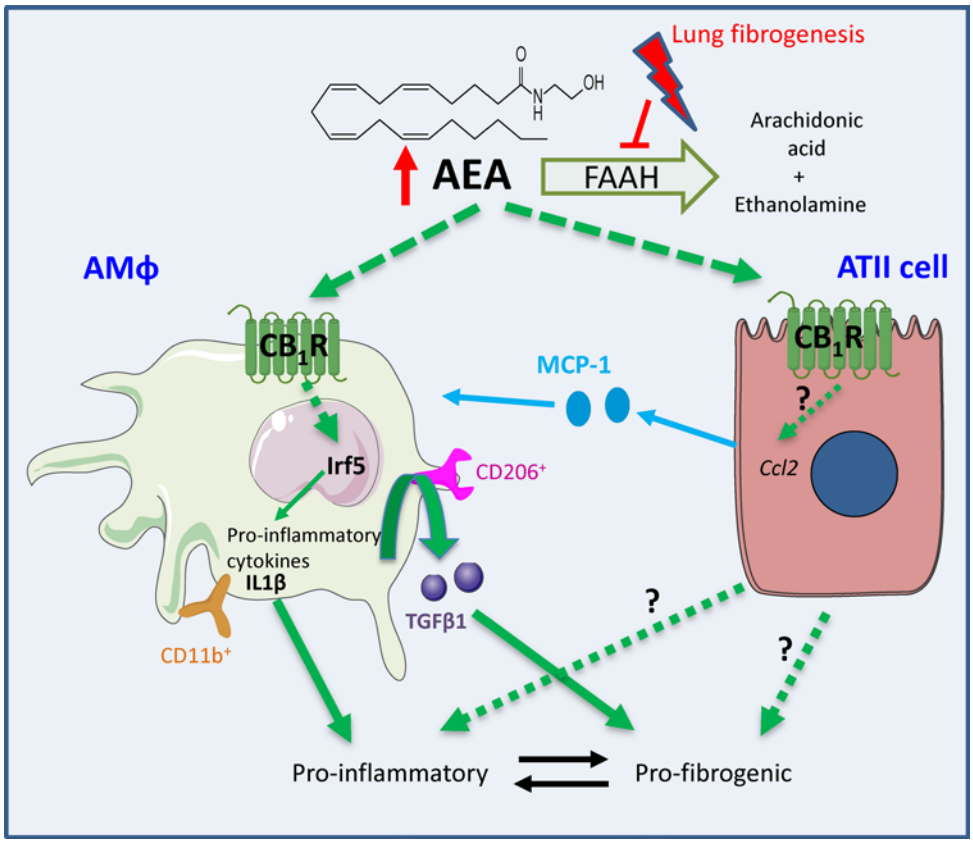

Figure 12. Schematic representation of the overactive endocannabinoid/CB_1R system and the proposed mechanisms of its proinflammatory and profibrotic functions in the lung. This figure was prepared using a template on ChemDraw Professional 15 (PerkinElmer Informatics) and the Servier medical art website (http://www.servier.fr/servier-medical-art). AEA, anandamide; AMφ, alveolar macrophage; ATII, alveolar type 2 epithelial cell.

Epithelial cells in various tissues may also respond to injury by increasing the cellular levels of AEA (30, 61). Thus, multiple cell types may contribute to the increase in AEA levels and CB_1R expression in the fibrotic lung, which warrants further studies. As for iNOS, its elevated activity induces nitrosative stress via reactive nitrogen species, which eventually promotes epithelial tissue injury. iNOS expression in ATII cells increases BL-PF (11). In agreement with previous studies, we observed increased expression and activity of iNOS in lung tissue with both experimental and clinical PF (11, 62). *Nos2*$^{-/-}$ mice displayed lower levels of fibrosis than WT mice after bleomycin challenge (Figure 5), in agreement with published findings (11, 15); this also suggested that pharmacological inhibition of iNOS has therapeutic benefit in PF (14, 15). Our finding that combined inhibition of CB_1R and iNOS results in greater antifibrotic efficacy than equivalent inhibition of CB_1R alone confirms this notion, and it also indicates that iNOS signals through targets not engaged by CB_1R.

Although we did not explore such targets in detail in the lung fibrosis model, we have previously reported that, in bile duct ligation–induced liver fibrosis, increased expression of the profibrogenic genes *Pdgfb*/*Pdgfrb* and *Nlrp3*/*Pycard* and integrin *αvβ6* was linked to increased iNOS but not CB_1R signaling (21), and these targets may also be uniquely engaged by iNOS in the lung. In the current study, CB_1R blockade or *Cnr1* deletion resulted in profound downregulation of the expression of another set of major profibrogenic genes, such as *Tgfb1*, *Ctgf*, *Pdgfc*, *Col1a*, *Fn1*, and *Timp1*, in the fibrotic lung, with no or much less pronounced decreases in the lungs of *Nos2*$^{-/-}$ mice (Figure 6A and Figure 10A). This suggests that the Tgfβ1 pathway may be a dominant target of CB_1R-mediated fibrogenesis in PF. The alveolar macrophages are a known source of Tgfβ1 that contributes to the profibrogenic milieu in the lung (63). In contrast to the preferential activation of fibrogenic gene expression by CB_1R over iNOS in the lungs of bleomycin-treated mice, iNOS activity was not significantly affected by *Cnr1* deletion, whereas it was absent in the *Nos2*$^{-/-}$ mice (Figure 7), suggesting corresponding differences in the degree of nitrosative stress. Thus, unique activation of distinct fibrogenic pathways by the two molecules likely accounts for the additive antifibrogenic effect resulting from their joint targeting for inhibition.

Although there are recently approved therapies available for IPF (see Introduction), they do not completely arrest progression of the disease. The limited success of medications with a single target suggests that multitargeted therapies may be more effective, considering the multifactorial pathology of IPF. Here, we report that a dual-target hybrid inhibitor of peripheral CB_1R and iNOS completely arrested the progression of BL-PF and dramatically improved the survival rate in a progression arrest treatment paradigm, providing proof of principle for a polypharmacology approach in this preclinical model of IPF. MRI-1867 is orally bioavailable and peripherally restricted to minimize the CNS liability observed in first-generation, brain-penetrant CB_1R antagonists. This and the favorable pharmacokinetic and druggable safety properties of this compound (21) should make it a viable candidate for future translational studies in IPF.

Methods

Chemicals. MRI-1867 was synthesized as described previously (21). Rimonabant was obtained from the National Institute of Drug Abuse Drug Supply Program (Research Triangle Park, North Carolina, USA). Fumonisin B was from Cayman. AM6545 was from Tocris. [^{14}C(U)]arginine was from Perkin-Elmer. Bleomycin (cell culture grade) and all the other chemicals were from Sigma-Aldrich.

Pulmonary function tests for human subjects. Pulmonary function testing was performed as described previously (64). Briefly, forced vital capacity, total lung capacity, and diffusion capacity of carbon monoxide measurements were performed in accordance with guidelines from the American Thoracic Society (SensorMedics). Values were expressed as percentages of predicted values.

BALF and lung tissue procurement for human subjects. BALF was isolated and lung tissue fixed in 10% formalin was procured as described previously (65, 66).

Endocannabinoid measurement. The tissue levels of endocannabinoids were measured by stable isotope dilution liquid chromatography/tandem mass spectrometry (LC-MS/MS) as described previously (67).

Animals. Eight- to ten-week-old male C57BL/6J mice were obtained from The Jackson Laboratory. *Cnr1*$^{-/-}$ mice were generated as described previously (68). *Nos2*$^{-/-}$ mice were purchased from The Jackson Laboratory. *Cnr1*$^{-/-}$ and *Nos2*$^{-/-}$ mice were on a C57Bl/6J genetic background. Mice were maintained under a 12-hour-light/12-hour-dark cycle and fed ad libitum. Mice were kept on a standard laboratory diet (NIH-31 rodent diet; Teklad NIH-31, Envigo).

Oropharyngeal aspiration of bleomycin. We used a BL-PF model by delivering bleomycin via oropharyngeal aspiration as previously defined (69), with slight modifications. Briefly, mice were anesthetized with intraperitoneal injection of ketamine/xylazine (84 mg/ml ketamine/1 ml/kg xylazine) and placed on a surgery board in the supine position at an angle of 45°, with the head immobilized by an elastic band across the upper incisors. Using a sterile forceps, the mouth was then nudged open and the tongue was gently pulled out and toward the mandible and lower incisors. This maneuver allowed visualization of the vocal cords under adequate lighting. Lidocaine gel (2%) was applied topically by a cotton swab to numb the vocal cords and thus prevent their spasm, which could cause dyspnea or choking. Bleomycin (1 U/kg) was delivered through the oropharynx using a sterile 100-μl pipette during inspiration at a volume of 100 μl/50 g body weight. Sterile saline was used as vehicle and applied to the control groups. The animals were then allowed to recover from the anesthesia.

Survival analysis for mice. Survival curves were plotted by using GraphPad Prism 6 software. Survival was analyzed by using log-rank (Mantel-Cox) test for assessing statistical difference between animal groups.

BALF and BAL cell harvesting from mice. BALF was collected from anesthetized mice by lavaging lungs 3 times with 0.5 ml Hanks' balanced salt solution without calcium and magnesium (HBS-) (Sigma-Aldrich). Then, collected BALF was diluted 2-fold by adding 1.5 ml HBSS-. BAL cells were collected by centrifuge at 500 *g* for 7 minutes at 4°C. Supernatant was collected as BALF for further analysis, and 100 μl BALF was subjected to endocannabinoid measurements. BAL cells were further used for either gene expression analysis or flow cytometry experiments.

BAL cell preparation and flow cytometry experiments. Collected BAL cells were resuspended in 1 ml PBS containing 0.5% bovine serum albumin (0.5%BSA-PBS) and centrifuged at 500 *g* for 7 minutes at 4°C. 300 μl ACK lysis buffer (Lonza) was added to the resulting pellet and incubated for 15 minutes at 37°C to remove red blood cells. The cell suspension was washed twice with 3 ml 0.5%BSA-PBS by centrifuging at 500 *g* for 7 minutes at 4°C. The resulting pellet was suspended in 1 ml 0.5%BSA-PBS, and the total number of the BAL cells was established by counting cells under a microscope. The cells were preincubated with Mouse BD Fc Block (purified rat anti-mouse CD16/CD32 [2.4G2] [catalog 553142]; BD Biosciences) at 4°C for 15 minutes and then stained with APC-conjugated anti-CD11b (catalog 101212), APC-conju-

gated anti-CD206 (catalog 141708), PerCP-conjugated anti-F4/80 (catalog 123126), PE-conjugated anti-CD68 (catalog 137014), FITC-conjugated anti-CD11c (catalog 117306), PE-conjugated anti-GR-1 (catalog 108408), and PE-conjugated anti-Nk1.1 (catalog 108707) (all from BioLegend) and FITC-conjugated anti-CD19 (catalog 557398) and APC-conjugated anti-CD4 (catalog 553051) (both from BD Biosciences Pharmingen) for 30 minutes at 4°C. The cells were centrifuged twice at 500 *g* for 7 minutes at 4°C. Then, the stained cells were fixed by adding 100 μl PBS containing 1% paraformaldehyde. The gating strategies for neutrophils, alveolar macrophages, and lymphocytes are shown in Supplemental Figure 4. For instance, following autofluorescence of BAL cells, alveolar macrophages were assessed using unstained cells, and alveolar macrophages were then defined as a autofluorescence-positive, F4/80^{dim}, CD11c-positive population (Auto^{+}F4/80^{dim}CD11c^{+}) (Supplemental Figure 3). Flow cytometry analysis was performed using FACSCalibur (BD Biosciences) and analyzed with FlowJo software (TreeStar).

Real-time PCR analyses. RNA extraction was performed using RNeasy Mini Kits from Qiagen. One microgram of total RNA was reverse transcribed to cDNA using the Bio-Rad iScript cDNA synthesis kit. Expression of the target gene was quantified with gene-specific primers and PowerSYBRGreen master mix using a StepOnePlus Real-Time PCR instrument from Applied Biosystems. Predesigned mouse *Tbp* (QT00198443), *Tgfb1* (QT00145250), *Ctgf* (QT00096131), *Pdgfc* (QT00170163), *Col1a* (QT00162204), *Fn1* (QT00135758), *Timp1* (QT00996282), *Ccl2* (QT00167832), *Cxcl12* (QT00161112), *Arg1* (QT00134288), *Nos2* (QT00100275), *Cnr1* (QT00115395), and *Irf5* (QT00252623) primers were purchased from Qiagen. The housekeeping gene TATA-Box Binding Protein (*Tbp*) was used as loading control. Gene expression values were calculated based on the ΔΔCt method.

Chemokine measurements. Lung levels of MCP-1 and CXCL12 abundance were measured using the CCL2 or CXCL12 mouse quantikine ELISA Kits, respectively (R&D Systems).

Drug treatment. The compounds were administered by oral gavage once daily as indicated. Vehicle was used at ratio of DMSO/Tween 80/saline (1:1:18). Oral formulations were applied at 1 mg/ml or 0.3 mg/ml concentrations to achieve doses of 10 or 3 mg/kg, respectively.

Tissue levels of drugs. MRI-1867 levels were measured by LC-MS/MS as described previously (21).

Radioisotopic iNOS activity assay. iNOS activity in lung tissue was performed as described previously (21).

Hydroxyproline measurement. The degree of lung fibrosis was quantified biochemically by measuring hydroxyproline content of lung extracts using LC-MS/MS as described previously (21). The left lung was excised, wet tissue weight was recorded, and the tissue was snap frozen in liquid nitrogen and kept at –80°C until use. Lung tissue was homogenized in 0.1 N perchloric acid (PCA) at a ratio of 100 mg/ml. Then, an equal volume of 12 N HCL was added, and the homogenate was hydrolyzed at 100°C for 4 hours. Hydrolyzed samples were vortexed and centrifuged at 10,000 *g* for 10 minutes, and 5 μl hydrolysate was diluted 200-fold by the addition of 995 μl of 0.1 N PCA. The hydroxyproline level was analyzed by LC-MS/MS under conditions described earlier (21). Values are expressed as nmol/left lung.

Histology and immunohistochemistry. The right lung was used for histology. During lung harvesting, first the left bronchial arm was ligated and the left lung was removed for biochemical analyses. The remaining right lung was then inflated by 1.5 ml of 10% neutralized formalin solution introduced into the trachea using a syringe. The right bronchial arm was then ligated to keep the lung inflated before its removal. The right lung was then fixed in 10% neutralized formalin solution, embedded in paraffin, and sectioned (4 μm) onto glass slides. Immunohistochemistry was performed as described previously (21) by using primary antibodies against iNOS (Abcam, 15323), CB_1R (anti-mouse L15) (70), SP-C (Santa Cruz Biotechnology, sc-7705), CD68 (Abcam, 31630), and α-SMA (Abcam 7817). For fluorescence detection, secondary antibodies coupled to Alexa Fluor 488 or Alexa Fluor 555 were used and sections were analyzed using a Zeiss LSM700 confocal microscope. Immunostaining intensity was quantified by using ImageJ software (NIH Public Domain) by a person blind to the sample ID. Quantification of images from one sample was averaged for actual data presentation for each sample (n = 6 per group).

Masson's trichrome staining. Histological staining was performed using Masson's Trichrome Kit (Thermo Fisher Scientific) with a slight optimization of the supplier's microwave staining protocol. 4-μm tissue sections were stained with the following time adjustments: DI water rinse adjusted to 5 minutes after Bouin's Fluid (Thermo Fisher Scientific); Weigert's Iron Hematoxylin stain adjusted to 3 minutes; Biebrich Scarlet-Acid Fuchsin solution adjusted to 2 minutes; and Aniline Blue Solution adjusted to 25 minutes. All other steps were performed as instructed by the manufacturer.

Ashcroft scoring. Images were taken at ×200 magnification from at least 8 randomly selected areas per

lung tissue slide. Three readers scored the same fields independently (0 = no fibrosis; 8 = severe fibrosis) and were blinded to study group.

Statistics. Statistical analysis was performed by unpaired 2-tailed Student's *t* test or by 1-way ANOVA, as appropriate and indicated in figure legends. $P < 0.05$ was considered significant.

Study approval. Subjects with IPF and healthy research volunteers provided written informed consent and enrolled in protocol 04-HG-0211, "Specimen Procurement for Individuals with Pulmonary Fibrosis," which was approved by the Institutional Review Board of the National Human Genome Research Institute. Study eligibility criteria were previously described (71). All animal procedures were approved by the Institutional Animal Care and Use Committee of NIAAA, NIH, and the experiments were carried out in accordance with the accepted guidelines.

Author contributions

RC planned and performed in vivo and in vitro experiments, analyzed data, and participated in manuscript preparation. BRG obtained clinical samples and performed pulmonary function tests. MRI designed, synthesized, and chemically analyzed MRI-1867. TY and TJ performed flow cytometry experiments. TJ, RC, JKP, and NJC performed histology and immunohistochemistry and prepared images. RC, GS, NJC, and JKP contributed to in vivo experiments. JKP, NJC, and ZL performed PCR and real-time PCR. BRG, TY, and HP performed Ashcroft scoring. KM contributed the CB_1R antibody and edited the manuscript. BRG, TY, and WAG participated in manuscript preparation. RC and GK designed the study, interpreted data, and wrote the manuscript. All authors had access to the manuscript and agreed with the final version.

Acknowledgments

This work was supported by the Intramural Research Programs of the NIAAA (to RC and GK), the American Thoracic Society Foundation Research Program and the Hermansky-Pudlak Syndrome Network (to RC), the National Institute on Drug Abuse (to KM, DA021696), and the National Human Genome Research Institute (to WAG). We thank Judith Harvey-White (NIAAA/NIH) for technical assistance. We thank Grzegorz Godlewski for his critical reading and comments.

Address correspondence to: Resat Cinar, Laboratory of Physiologic Studies, National Institute on Alcohol Abuse and Alcoholism, NIH, 5625 Fishers Lane, Room 2S-18, Rockville, Maryland 20852, USA. Phone: 301.443.4098; E-mail: resat.cinar@nih.gov.

GS's present address is: Department of Physiology, Faculty of Medicine, Semmelweis University, Budapest, Hungary.

1. Friedman SL, Sheppard D, Duffield JS, Violette S. Therapy for fibrotic diseases: nearing the starting line. *Sci Transl Med*. 2013;5(167):167sr1.
2. Lu JJ, Pan W, Hu YJ, Wang YT. Multi-target drugs: the trend of drug research and development. *PLoS One*. 2012;7(6):e40262.
3. Idiopathic Pulmonary Fibrosis Clinical Research Network, Raghu G, Anstrom KJ, King TE, Lasky JA, Martinez FJ. Prednisone, azathioprine, and N-acetylcysteine for pulmonary fibrosis. *N Engl J Med*. 2012;366(21):1968–1977.
4. King TE, et al. A phase 3 trial of pirfenidone in patients with idiopathic pulmonary fibrosis. *N Engl J Med*. 2014;370(22):2083–2092.
5. Richeldi L, et al. Efficacy and safety of nintedanib in idiopathic pulmonary fibrosis. *N Engl J Med*. 2014;370(22):2071–2082.
6. Bolognesi ML. Polypharmacology in a single drug: multitarget drugs. *Curr Med Chem*. 2013;20(13):1639–1645.
7. Ricciardolo FL, Di Stefano A, Sabatini F, Folkerts G. Reactive nitrogen species in the respiratory tract. *Eur J Pharmacol*. 2006;533(1-3):240–252.
8. Bargagli E, Olivieri C, Bennett D, Prasse A, Muller-Quernheim J, Rottoli P. Oxidative stress in the pathogenesis of diffuse lung diseases: a review. *Respir Med*. 2009;103(9):1245–1256.
9. Kalayarasan S, Sriram N, Sudhandiran G. Diallyl sulfide attenuates bleomycin-induced pulmonary fibrosis: critical role of iNOS, NF-kappaB, TNF-alpha and IL-1beta. *Life Sci*. 2008;82(23-24):1142–1153.
10. Naura AS, et al. Requirement for inducible nitric oxide synthase in chronic allergen exposure-induced pulmonary fibrosis but not inflammation. *J Immunol*. 2010;185(5):3076–3085.
11. Pullamsetti SS, et al. The role of dimethylarginine dimethylaminohydrolase in idiopathic pulmonary fibrosis. *Sci Transl Med*. 2011;3(87):87ra53.
12. Romanska HM, et al. iNOS gene upregulation is associated with the early proliferative response of human lung fibroblasts to cytokine stimulation. *J Pathol*. 2002;197(3):372–379.
13. Parra ER, Aguiar Junior AC, Silva LO, Souza HS, Espinoza JD, Capelozzi VL. Morphometric evaluation of nitric oxide synthase isoforms and their cytokine regulators predict pulmonary dysfunction and survival in systemic sclerosis. *Braz J Med Biol*

Res. 2013;46(10):881–891.
14. Giri SN, Biring I, Nguyen T, Wang Q, Hyde DM. Abrogation of bleomycin-induced lung fibrosis by nitric oxide synthase inhibitor, aminoguanidine in mice. *Nitric Oxide*. 2002;7(2):109–118.
15. Genovese T, et al. Inhibition or knock out of inducible nitric oxide synthase result in resistance to bleomycin-induced lung injury. *Respir Res*. 2005;6:58.
16. Pacher P, Kunos G. Modulating the endocannabinoid system in human health and disease--successes and failures. *FEBS J*. 2013;280(9):1918–1943.
17. Teixeira-Clerc F, et al. CB1 cannabinoid receptor antagonism: a new strategy for the treatment of liver fibrosis. *Nat Med*. 2006;12(6):671–676.
18. Patsenker E, et al. Cannabinoid receptor type I modulates alcohol-induced liver fibrosis. *Mol Med*. 2011;17(11-12):1285–1294.
19. Trebicka J, et al. Role of cannabinoid receptors in alcoholic hepatic injury: steatosis and fibrogenesis are increased in CB2 receptor-deficient mice and decreased in CB1 receptor knockouts. *Liver Int*. 2011;31(6):860–870.
20. Reichenbach V, et al. Prevention of fibrosis progression in CCl4-treated rats: role of the hepatic endocannabinoid and apelin systems. *J Pharmacol Exp Ther*. 2012;340(3):629–637.
21. Cinar R, et al. Hybrid inhibitor of peripheral cannabinoid-1 receptors and inducible nitric oxide synthase mitigates liver fibrosis. *JCI Insight*. 2016;1(11):e87336.
22. Lin CL, et al. Cannabinoid receptor 1 disturbance of PPARγ2 augments hyperglycemia induction of mesangial inflammation and fibrosis in renal glomeruli. *J Mol Med*. 2014;92(7):779–792.
23. Lecru L, et al. Cannabinoid receptor 1 is a major mediator of renal fibrosis. *Kidney Int*. 2015;88(1):72–84.
24. Slavic S, et al. Cannabinoid receptor 1 inhibition improves cardiac function and remodelling after myocardial infarction and in experimental metabolic syndrome. *J Mol Med*. 2013;91(7):811–823.
25. Lazzerini PE, et al. Adenosine A2A receptor activation stimulates collagen production in sclerodermic dermal fibroblasts either directly and through a cross-talk with the cannabinoid system. *J Mol Med*. 2012;90(3):331–342.
26. Bronova I, et al. Protection from radiation-induced pulmonary fibrosis by peripheral targeting of cannabinoid receptor-1. *Am J Respir Cell Mol Biol*. 2015;53(4):555–562.
27. Jourdan T, et al. Activation of the Nlrp3 inflammasome in infiltrating macrophages by endocannabinoids mediates beta cell loss in type 2 diabetes. *Nat Med*. 2013;19(9):1132–1140.
28. Jourdan T, et al. Developmental Role of Macrophage Cannabinoid-1 Receptor Signaling in Type 2 Diabetes. *Diabetes*. 2017;66(4):994–1007.
29. Liu D, Darville M, Eizirik CL. Double-Stranded Ribonucleic Acid (RNA) Induces β-Cell Fas Messenger RNA Expression and Increases Cytokine-Induced β-Cell Apoptosis. *Endocrinology*. 2001;142(6):2593–2599.
30. Osei-Hyiaman D, et al. Endocannabinoid activation at hepatic CB1 receptors stimulates fatty acid synthesis and contributes to diet-induced obesity. *J Clin Invest*. 2005;115(5):1298–1305.
31. Rouhani FN, et al. Alveolar macrophage dysregulation in Hermansky-Pudlak syndrome type 1. *Am J Respir Crit Care Med*. 2009;180(11):1114–1121.
32. Tam J, et al. Peripheral CB1 cannabinoid receptor blockade improves cardiometabolic risk in mouse models of obesity. *J Clin Invest*. 2010;120(8):2953–2966.
33. Alzaid F, et al. IRF5 governs liver macrophage activation that promotes hepatic fibrosis in mice and humans. *JCI Insight*. 2016;1(20):e88689.
34. Saigusa R, et al. Multifaceted contribution of the TLR4-activated IRF5 transcription factor in systemic sclerosis. *Proc Natl Acad Sci USA*. 2015;112(49):15136–15141.
35. Rice W, Shannon JM, Burton F, Fiedeldey D. Expression of a brain-type cannabinoid receptor (CB1) in alveolar type II cells in the lung: regulation by hydrocortisone. *Eur J Pharmacol*. 1997;327(2-3):227–232.
36. Calignano A, et al. Bidirectional control of airway responsiveness by endogenous cannabinoids. *Nature*. 2000;408(6808):96–101.
37. Staiano RI, et al. Human lung-resident macrophages express CB1 and CB2 receptors whose activation inhibits the release of angiogenic and lymphangiogenic factors. *J Leukoc Biol*. 2016;99(4):531–540.
38. Mehrad B, Burdick MD, Zisman DA, Keane MP, Belperio JA, Strieter RM. Circulating peripheral blood fibrocytes in human fibrotic interstitial lung disease. *Biochem Biophys Res Commun*. 2007;353(1):104–108.
39. Bogatkevich GS, Ludwicka-Bradley A, Singleton CB, Bethard JR, Silver RM. Proteomic analysis of CTGF-activated lung fibroblasts: identification of IQGAP1 as a key player in lung fibroblast migration. *Am J Physiol Lung Cell Mol Physiol*. 2008;295(4):L603–L611.
40. Ekert JE, Murray LA, Das AM, Sheng H, Giles-Komar J, Rycyzyn MA. Chemokine (C-C motif) ligand 2 mediates direct and indirect fibrotic responses in human and murine cultured fibrocytes. *Fibrogenesis Tissue Repair*. 2011;4(1):23.
41. Mercer PF, et al. Pulmonary epithelium is a prominent source of proteinase-activated receptor-1-inducible CCL2 in pulmonary fibrosis. *Am J Respir Crit Care Med*. 2009;179(5):414–425.
42. Pan LH, et al. Type II alveolar epithelial cells and interstitial fibroblasts express connective tissue growth factor in IPF. *Eur Respir J*. 2001;17(6):1220–1227.
43. Moeller A, et al. Circulating fibrocytes are an indicator of poor prognosis in idiopathic pulmonary fibrosis. *Am J Respir Crit Care Med*. 2009;179(7):588–594.
44. Young LR, et al. Epithelial-macrophage interactions determine pulmonary fibrosis susceptibility in Hermansky-Pudlak syndrome. *JCI Insight*. 2016;1(17):e88947.
45. Wynn TA, Vannella KM. Macrophages in tissue repair, regeneration, and fibrosis. *Immunity*. 2016;44(3):450–462.
46. Byrne AJ, Maher TM, Lloyd CM. Pulmonary Macrophages: A New Therapeutic Pathway in Fibrosing Lung Disease? *Trends Mol Med*. 2016;22(4):303–316.
47. Pechkovsky DV, et al. Alternatively activated alveolar macrophages in pulmonary fibrosis-mediator production and intracellular signal transduction. *Clin Immunol*. 2010;137(1):89–101.
48. Zaynagetdinov R, et al. Identification of myeloid cell subsets in murine lungs using flow cytometry. *Am J Respir Cell Mol Biol*. 2013;49(2):180–189.

49. Hussell T, Bell TJ. Alveolar macrophages: plasticity in a tissue-specific context. *Nat Rev Immunol*. 2014;14(2):81–93.
50. Weiss M, Blazek K, Byrne AJ, Perocheau DP, Udalova IA. IRF5 is a specific marker of inflammatory macrophages in vivo. *Mediators Inflamm*. 2013;2013:245804.
51. Weiss M, et al. IRF5 controls both acute and chronic inflammation. *Proc Natl Acad Sci USA*. 2015;112(35):11001–11006.
52. Liu J, et al. Lipopolysaccharide induces anandamide synthesis in macrophages via CD14/MAPK/phosphoinositide 3-kinase/NF-kappaB independently of platelet-activating factor. *J Biol Chem*. 2003;278(45):45034–45039.
53. Maccarrone M, et al. Lipopolysaccharide downregulates fatty acid amide hydrolase expression and increases anandamide levels in human peripheral lymphocytes. *Arch Biochem Biophys*. 2001;393(2):321–328.
54. Palumbo-Zerr K, et al. Inactivation of fatty acid amide hydrolase exacerbates experimental fibrosis by enhanced endocannabinoid-mediated activation of CB1. *Ann Rheum Dis*. 2012;71(12):2051–2054.
55. Liu J, et al. A biosynthetic pathway for anandamide. *Proc Natl Acad Sci USA*. 2006;103(36):13345–13350.
56. Matias I, Pochard P, Orlando P, Salzet M, Pestel J, Di Marzo V. Presence and regulation of the endocannabinoid system in human dendritic cells. *Eur J Biochem*. 2002;269(15):3771–3778.
57. Holt S, et al. Lipopolysaccharide-induced pulmonary inflammation is not accompanied by a release of anandamide into the lavage fluid or a down-regulation of the activity of fatty acid amide hydrolase. *Life Sci*. 2004;76(4):461–472.
58. Börner C, Höllt V, Sebald W, Kraus J. Transcriptional regulation of the cannabinoid receptor type 1 gene in T cells by cannabinoids. *J Leukoc Biol*. 2007;81(1):336–343.
59. Mukhopadhyay B, et al. Transcriptional regulation of cannabinoid receptor-1 expression in the liver by retinoic acid acting via retinoic acid receptor-gamma. *J Biol Chem*. 2010;285(25):19002–19011.
60. Jourdan T, Djaouti L, Demizieux L, Gresti J, Vergès B, Degrace P. CB1 antagonism exerts specific molecular effects on visceral and subcutaneous fat and reverses liver steatosis in diet-induced obese mice. *Diabetes*. 2010;59(4):926–934.
61. Jourdan T, et al. Overactive cannabinoid 1 receptor in podocytes drives type 2 diabetic nephropathy. *Proc Natl Acad Sci USA*. 2014;111(50):E5420–E5428.
62. Gurujeyalakshmi G, Wang Y, Giri SN. Suppression of bleomycin-induced nitric oxide production in mice by taurine and niacin. *Nitric Oxide*. 2000;4(4):399–411.
63. Kolahian S, Fernandez IE, Eickelberg O, Hartl D. Immune mechanisms in pulmonary fibrosis. *Am J Respir Cell Mol Biol*. 2016;55(3):309–322.
64. Gochuico BR, et al. Progressive preclinical interstitial lung disease in rheumatoid arthritis. *Arch Intern Med*. 2008;168(2):159–166.
65. Ren P, Rosas IO, Macdonald SD, Wu HP, Billings EM, Gochuico BR. Impairment of alveolar macrophage transcription in idiopathic pulmonary fibrosis. *Am J Respir Crit Care Med*. 2007;175(11):1151–1157.
66. Cullinane AR, et al. Dysregulation of galectin-3. Implications for Hermansky-Pudlak syndrome pulmonary fibrosis. *Am J Respir Cell Mol Biol*. 2014;50(3):605–613.
67. Cinar R, et al. Hepatic cannabinoid-1 receptors mediate diet-induced insulin resistance by increasing de novo synthesis of long-chain ceramides. *Hepatology*. 2014;59(1):143–153.
68. Zimmer A, Zimmer AM, Hohmann AG, Herkenham M, Bonner TI. Increased mortality, hypoactivity, and hypoalgesia in cannabinoid CB1 receptor knockout mice. *Proc Natl Acad Sci USA*. 1999;96(10):5780–5785.
69. Egger C, et al. Administration of bleomycin via the oropharyngeal aspiration route leads to sustained lung fibrosis in mice and rats as quantified by UTE-MRI and histology. *PLoS One*. 2013;8(5):e63432.
70. Bodor AL, et al. Endocannabinoid signaling in rat somatosensory cortex: laminar differences and involvement of specific interneuron types. *J Neurosci*. 2005;25(29):6845–6856.
71. El-Chemaly S, et al. Nuclear localization of vascular endothelial growth factor-D and regulation of c-Myc-dependent transcripts in human lung fibroblasts. *Am J Respir Cell Mol Biol*. 2014;51(1):34–42.